Targeting of integral membrane proteins to the perimeter of lipid droplets reveals a barrier function of FIT proteins

Rasha Khaddaj[1], Muriel Mari[2], Stéphanie Cottier[1], Fulvio Reggiori[2], and Roger Schneiter[1*]

[1]Department of Biology, University of Fribourg, Chemin du Musée 10, 1700 Fribourg, Switzerland

[2]Department of Biomedical Sciences of Cells and Systems, University of Groningen, University Medical Center Groningen, A. Deusinglaan 1, 9713 AV Groningen, Netherlands

Short title: Targeting of membrane proteins to lipid droplets

Key words: Lipid droplets, endoplasmic reticulum, *Saccharomyces cerevisiae*, perilipins, Seipin, triacylglycerol

*Corresponding author: Roger Schneiter, Division of Biochemistry, Department of Biology, University of Fribourg, Chemin du Musée 10, 1700 Fribourg, Switzerland, Phone +41 26 300 8654, Email: roger.schneiter@unifr.ch

Abstract

Lipid droplets (LDs) constitute globular subcellular structures that mainly serve to store energy in form of neutral lipids, particularly triacylglycerol and steryl esters. LDs are closely associated with the membrane of the endoplasmic reticulum (ER), and are limited by a monolayer membrane of phospholipids harboring a specific set of proteins. Most of these proteins associate with LDs through either an amphipathic helix or a membrane-embedded hairpin motif. Here we address the question whether integral membrane proteins could localize to the surface of LDs. To test this, we fused perilipin 3 (PLIN3), a mammalian LD-targeted protein, to ER resident proteins, such as Wbp1 (a N-glycosyl transferase complex subunit), Sec61 (a translocon subunit), and Pmt1 (a protein O-mannosyltransferase). The resulting fusion proteins localize to the rim of LDs in both yeast and mammalian cells. LD targeting of membrane proteins is not only observed with the PLIN3-containing fusion proteins, but also for native endogenous polytopic transmembrane proteins. These data indicate that integral membrane proteins that function in a bilayer membrane can reversibly associate with the LD surface, suggesting that the LD surface is continuous with the ER membrane. In cells lacking LDs, Wbp1 and Sec61 fusion proteins localize to the ER, forming crescent-like membrane protrusions. These ER crescents resemble sites of LD formation as they contain seipin and other LD-localized proteins, suggesting that membrane-anchored PLIN3 induces the formation of membrane subdomains.

Introduction

Lipid droplets (LDs) are present in most cells, where they are discernible as globular structures. Adipocytes typically contain few large unilocular LDs, whereas other cells, such as yeast may contain up to a dozen of distinct LDs that are relatively small in size. LDs are mostly composed of neutral lipids, particularly triacylglycerol (TAG) and steryl esters (STE). This hydrophobic core of neutral lipids is surrounded by a phospholipid monolayer that harbors a specific set of proteins, many of which function in neutral lipid metabolism, such as lipases or acyltransferases. The morphology of LDs is somewhat reminiscent of that of apolipoproteins and milk globules, but unlike these structures, LDs are not secreted. LDs serve to store metabolic energy, which is released upon beta-oxidation of fatty acids esterified to these neutral lipids. In addition, lipids stored in LDs can also serve as readily available building blocks for rapid membrane proliferation. Thus, LDs can buffer both an excess and a lack of fatty acids, and thereby provide a protective role in lipotoxicity. Hence, LD homeostasis is associated with multiple prevalent human diseases including obesity and atherosclerosis (Thiam *et al.*, 2013; Walther *et al.*, 2017; Olzmann and Carvalho, 2018; Thiam and Dugail, 2019).

The biogenesis of LDs is driven by the formation of neutral lipids by endoplasmic reticulum (ER)-resident acyltransferases. Accordingly, the current model postulates that LDs originate from the ER membrane, where the accumulation of neutral lipids leads to the formation of lens-like structures within the ER bilayer. Growth of these neutral lipid lenses drives the formation of nascent LDs, which eventually emerge from the ER as mature LDs (Murphy and Vance, 1999). Key aspects of this conceptual model are now starting to become supported by experimental evidence. For example, molecular modeling of neutral lipids in a bilayer membrane indicates that neutral lipids nucleate to form lens-like structures (Khandelia *et al.*, 2010; Thiam and Forêt, 2016). In addition, functional studies revealed that the activation of fatty acids and their incorporation into TAG occurs at specific ER microdomains from where LDs emerge (Xu *et al.*, 2012; Kassan *et al.*, 2013). Finally, the induction of neutral lipid synthesis in yeast has indicated that LD-like structures initially form in the ER membrane (Jacquier *et al.*, 2011; Choudhary *et al.*, 2015). In both yeast and mammalian cells, LDs appear to stay in close association with the ER membrane, allowing for the exchange of proteins and lipids between these two compartments (Zehmer *et al.*, 2009; Jacquier *et al.*, 2011; Kassan *et al.*, 2013; Wilfling *et al.*, 2013; Markgraf *et al.*, 2014).

The transfer of proteins and lipids between the ER and LDs is likely to occur through membrane contact sites (MCS) between the two compartments. These MCS are maintained by ER resident integral membrane proteins, including seipins and fat storage-inducing transmembrane (FIT) proteins, which are both required for proper LD biogenesis and modulate LD size and abundance (Szymanski *et al.*, 2007; Kadereit *et al.*, 2008). Members of the seipin protein family, which comprises human BSCL2 and yeast Fld1/Ldb16, form large oligomeric complexes at ER-LD MCS, and harbor an ER luminal lipid binding domain (Sui *et al.*, 2018; Yan *et al.*, 2018). Seipins have been proposed to act as a diffusion barrier at ER-LD MCS to uncouple the lipid composition of the ER membrane from that of LDs, thereby contributing to the establishment of LD identity (Grippa *et al.*, 2015; Salo *et al.*, 2016). FIT proteins, on the other hand, which include human FIT1 and FIT2, and yeast Scs3 and Yft2, bind TAG and diacylglycerol (DAG) *in vitro* (Gross *et al.*, 2011; Goh *et al.*, 2015). Lack of FIT proteins leads to the formation of LDs that remain enclosed in the ER, suggesting that these proteins function to promote cytoplasmic emergence of LDs (Choudhary *et al.*, 2015).

Proteins can target the surface of LDs either from the cytoplasmic space or through the ER membrane (Dhiman *et al.*, 2020). Soluble proteins, such as the abundant LD scaffolding perilipins (PLINs) and their yeast homologue Pet10, are cytosolic in the absence of LDs, but are recruited onto the surface of these organelles upon induction of their biogenesis (Brasaemle, 2007; Bulankina *et al.*, 2009; Jacquier *et al.*, 2013; Gao *et al.*, 2017). PLINs contain 11-mer amphipathic repeat segments similar to those present in apolipoproteins and the Parkinson's disease-associated alpha-synuclein. These amphipathic repeats are important for LD targeting (Rowe *et al.*, 2016; Gao *et al.*, 2017; Copic *et al.*, 2018, Nat Commun, 9, 1332). In general, these repeat segments are intrinsically unstructured, but adopt a helical structure upon binding to LDs, possibly by recognizing lipid packing defects at their surface (Mishra *et al.*, 1994; Bussell and Eliezer, 2003; Bulankina *et al.*, 2009; Prévost *et al.*, 2018).

LD-localized membrane proteins, on the other hand, are first inserted into the ER membrane from where they then redistribute to LDs (Kory *et al.*, 2016). In the absence of LDs, these proteins display uniform ER localization and biochemically behave as ER integral membrane proteins. They are characterized by a hairpin type of membrane topology (Zehmer *et al.*, 2009; Jacquier *et al.*, 2011; Kassan *et al.*, 2013; Wilfling *et al.*, 2013). However, how exactly such membrane-anchored proteins move from the ER bilayer membrane onto the phospholipid monolayer of LDs is not well understood.

Here, we address the question whether normal ER resident integral membrane proteins can be targeted to the surface of LDs. We generated chimeras between two well-characterized ER membrane proteins, Wbp1, a subunit of the oligosaccharyl transferase glycoprotein complex, and Sec61, a subunit of the ER translocon, and the perilipin, PLIN3, which contains the information to target a protein to LDs. The resulting fusion proteins are targeted to the periphery of LDs, in both yeast and mammalian cells. Targeting of these membrane proteins to LDs is reversible as they relocalize from LDs back to the ER under lipolytic conditions, i.e., when neutral lipids are consumed and LDs dissipate. Interestingly, in the absence of LDs, these membrane-anchored PLIN3 fusion proteins localize to the ER, where they form crescent-like protrusions. These crescents contain the LD biogenesis protein seipin and other LD marker proteins, suggesting that perilipins induce the formation of membrane domains resembling those of mature LDs. Targeting of integral membrane proteins from the ER to LDs is not only observed for PLIN3-containing fusion proteins but also for native endogenous membrane proteins, suggesting that the surface of LDs is continuous with the ER membrane.

Results

Targeting of integral membrane proteins to LDs

To test whether ER residential integral membrane proteins could be targeted to the surface of LDs, we chose two well-characterize ER resident proteins: Wbp1, a single spanning membrane protein and component of the oligosaccharyl transferase complex required for N-linked glycosylation of proteins in the ER lumen, and Sec61, a multispanning transmembrane protein and subunit of the ER translocon (Deshaies and Schekman, 1987; te Heesen *et al.*, 1992). Wbp1 and Sec61 were fused to a cassette consisting of a fluorescent reporter protein, GFP, and perilipin 3 (PLIN3/TIP47), a mammalian LD-localized protein (Wolins *et al.*, 2001; Bulankina *et al.*, 2009) (Fig. 1A). PLIN3 has previously been shown to localize to LDs when expressed in yeast and that it associates to LDs through its amphipathic helix (Jacquier *et al.*, 2013; Rowe *et al.*, 2016). The expression of these reporter constructs was placed under the control of a tetracycline regulatable promoter (Tet-Off) and expression was typically induced by depleting doxycycline from the medium during overnight growth of the cells (Garí *et al.*, 1997). The subcellular localization of these fusion proteins was then analyzed by

fluorescence microscopy. Both Wbp1-GFP-PLIN3 and Sec61-GFP-PLIN3 localized to punctate structures which were also stained with Nile Red, a LD specific dye (Fig. 1B). Colocalization was extensive since more than 86% of all GFP positive punctate structures were also stained with Nile Red (Fig. 1C). Decoration of LDs with these chimeras is not simply due to proteolytic cleavage of the GFP-PLIN3 reporter from the membrane anchor, as the fusion proteins were stable when analyzed by Western blotting and degradation intermediates could not be detected (Fig. 1F). These data indicate that integral membrane proteins can be localized to LDs.

We then grew cells in presence of oleic acid to increase the number and size of LDs. Both reporter constructs, Wbp1-GFP-PLIN3 and Sec61-GFP-PLIN3 localized to the limiting membrane of LDs and perfectly colocalized with the LD marker protein Erg6-mCherry (Fig. 1D). This colocalization pattern was observed in more than 90% of the LDs (Fig. 1E).

To substantiate this result, we subsequently performed a membrane flotation assay. We found that Wbp1-GFP-PLIN3 and Sec61-GFP-PLIN3 chimeras were enriched in the subcellular fraction containing LDs obtained by flotation, as was Ayr1, an LD marker protein (Athenstaedt and Daum, 2000) (Fig. 1G). Subcellular fractionation also indicated that these two constructs remained membrane-anchored despite their fusion to GFP and PLIN3. They were enriched in a microsomal membrane pellet fraction (P13 and P30) as were endogenous Wbp1 and Sec61 (Fig. 1H). Thus, we conclude that the appendage of PLIN3 as an LD-targeting tag to Wbp1 and Sec61, does not affect their property to fractionate with microsomal membranes. Importantly, both fusion proteins stayed membrane-anchored upon treatment of the microsomal membranes with 1 M salt or carbonate, but they became solubilized upon detergent treatment with 1% SDS, displaying the same membrane association properties as did endogenous Wbp1 and Sec61 (Fig. 1I). In addition, treatment of microsomal membranes with endoglycosidase H, resulted in a mobility shift of both the Wbp1-based chimera and native Wbp1, suggesting that the chimeric protein is glycosylated in its large ER luminal domain (Fig. 1J). Altogether, these results show that the generated fusion proteins conserved the biochemical properties of integral membrane proteins and their original topology, despite their localization at the rim of LDs.

Wbp1-GFP-PLIN3 and Sec61-GFP-PLIN3 induce a local ER reorganization adjacent to LDs

To examine whether the localization of Wbp1-GFP-PLIN3 and Sec61-GFP-PLIN3 to LDs alter somehow the morphology of this organelle, we then analyzed cells expressing Erg6-GFP, or one of the two chimeras at the ultrastructural level using immune-electron microscopy. As expected, Erg6-GFP specifically localized on the perimeter of LDs, and these organelles display MCS with the ER but also the vacuole (Fig. 2A). In cells expressing Wbp1-GFP-PLIN3, labelling was found on the surface of LDs but also within a vesicular-tubular network (Fig. 2B, red square). In addition, these cells displayed long stretches of ER in close proximity to LDs, covering >70% of the LD perimeter. This was a peculiarity of this strain as in Erg6-GFP or Sec61-PLIN3-GFP expressing cells, only 15-23% of the LD perimeter was in clear contact with the ER (Fig. 2D). LDs in cells expressing Sec61-GFP-PLIN3 displayed gold labelling over their limiting membrane and frequent MCS with both the ER and the vacuoles (Fig. 2C). These ultrastructural observations confirm the confocal microscopy results, i.e., the Wbp1-GFP-PLIN3 and Sec61-GFP-PLIN3 chimeras are specifically recruited on the surface of LDs and, particularly in cells expressing Wbp1-GFP-PLIN3, they also enhance the presence of ER-LD MCS. Such extensive ER-LD contacts have previously been observed in cells cultivated in oleic acid-containing medium, which enhanced LD production at the expense of phospholipid synthesis, particularly that of phosphatidylinositol (Chorlay *et al.*, 2019).

Integral membrane proteins can be targeted to LDs in mammalian cells

Given that targeting of amphipathic helices to LDs is conserved among fungal, plant and animal cells, we tested whether mammalian ER membrane proteins could also be localized to LDs. Therefore, we created chimeric constructs composed of mammalian ER membrane proteins fused to GFP-PLIN3. As ER membrane proteins, we chose OST48, a single spanning ER protein and a subunit of the mammalian oligosaccharyl transferase complex (Roboti and High, 2012), and SEC61A1, a multispanning ER protein and component of the mammalian translocon (Görlich *et al.*, 1992). When transfected into HEK293 cells, OST48-GFP-PLIN3, SEC61A1-GFP-PLIN3, and GFP-PLIN3 all localized to punctate structures that were stained by Nile Red (Fig. 3A). These three chimeras also colocalized with mCherry-PLIN2 at the surface of LDs (Fig. 3B). Colocalization of the chimeric fusion proteins with either Nile Red or mCherry-PLIN2 was typically >81%, irrespective of whether the cells were treated with oleic acid or not (Fig. 3C, D). Taken together, these data indicate that

integral ER membrane proteins can also be targeted to the LD periphery in mammalian cells as well, suggesting that the interface between the ER and LDs is functionally conserved among eukaryotes.

LDs containing Wbp1-GFP-PLIN3 or Sec61-GFP-PLIN3 are functional in neutral lipid synthesis and mobilization

Cells store neutral lipids in LDs during times of energy excess and they degrade them to harvest energy or lipid components for membrane expansion. To examine whether the membrane-anchored PLIN3-based reporters impact these LD functions, we tested whether cells display defects in neutral lipid storage and mobilization when expressing Wbp1-GFP-PLIN3 or Sec61-GFP-PLIN3. Cells were grown in the presence of [^{3}H]palmitic acid for short periods of time and the incorporation of this radiolabeled fatty acid into TAG and STE was monitored by thin layer chromatography (TLC). Cells expressing Wbp1-GFP-PLIN3 or Sec61-GFP-PLIN3 synthesized TAG and STE with an efficiency similar to cells expressing the soluble GFP-PLIN3 (Fig. S1A). To analyze neutral lipid mobilization, cells were radiolabeled with [^{3}H]palmitic acid overnight and then treated with cerulenin and terbinafine, to simultaneously inhibit fatty acid and sterol synthesis. Under these conditions, cells hydrolyze their neutral lipid pool (Köffel *et al.*, 2005). While STE turnover occurred with similar efficiency in cells expressing either Wbp1-GFP-PLIN3 or Sec61-GFP-PLIN3, there were slight differences in TAG mobilization between these cells, with Sec61-GFP-PLIN3 displaying the slowest rate of TAG mobilization (Fig. S1B). Taken together, these data indicate that LDs are functional for both lipogenesis and lipolysis in cells expressing Wbp1-GFP-PLIN3 or Sec61-GFP-PLIN3, suggesting that the presence of these reporters does not impair the synthesis and transfer of neutral lipids between LDs and the ER membrane.

Dga1, a TAG synthase that is anchored to the ER membrane through a hairpin type of topology, relocalizes from the ER to LDs upon maturation of LDs, and moves back to the ER again upon neutral lipid mobilization, suggesting continuity between the two compartments (Jacquier *et al.*, 2011). We next wondered whether the membrane-anchored reporters would behave similarly. Mobilization of neutral lipids was therefore induced in cells coexpressing the ER marker mCherry-HDEL and Dga1-GFP, Wbp1-GFP-PLIN3 or Sec61-GFP-PLIN3. Already after 2 h of cerulenin treatment to induce lipolysis, Dga1-GFP substantially redistributed to the ER (Fig. S1C). Sec61-GFP-PLIN3 displayed crescent-like ER localization after 2, 4 and 6 h of

cerulenin treatment (Fig. S1C). Wbp1-GFP-PLIN3, in contrast, continued to display a punctate localization even after 6 h of cerulenin-induced lipolysis, showing that this chimera does not disperse back into the ER membrane upon LD shrinkage (Fig. S1C). This might be explained by the fact that Wbp1 forms part of a very large membrane protein complex, the oligosaccharyl transferase, which consist of eight subunits in yeast and might be too large and immobile to move back to the ER (Wild *et al.*, 2018). The observation that Sec61-GFP-PLIN3 disperses at least partially back into the ER membrane upon lipolysis, however, indicates that polytopic membrane proteins can relocalize back into the ER bilayer upon lipolytic consumption of LDs.

Wbp1-GFP-PLIN3 and Sec61-GFP-PLIN3 form crescent-like ER domains resembling sites of LD formation

Upon LD shrinkage, the membrane-anchored reporters partially relocalized back to the ER, where they accumulated in crescent-like protrusions (Fig. S1C). To examine whether these PLIN3-based reporters have a propensity to form membrane domains in the absence of neutral lipids, we analyzed their distribution in cells devoid of LDs. Cells bearing deletions of all four genes required for neutral lipid synthesis; *DGA1* and *LRO1* for TAG synthesis and *ARE1* and *ARE2* for STE synthesis are viable but lack LDs (Sandager *et al.*, 2002). In this quadruple mutant, both Wbp1-GFP-PLIN3 and Sec61-GFP-PLIN3 displayed a patched, crescent-like, localization at the ER, as revealed by their partial colocalization with mCherry-HDEL, an ER luminal marker protein (Fig. 4A, B). These structures were also stained with Nile Red, indicating that they bear hallmarks of early stages of LD formation (Fig. 4C, D).

To further characterize the nature of the crescent-like ER domains formed by the membrane-anchored PLIN3 chimeras, we tested whether these protrusions would dissolve upon induction of LD formation. To this aim, we took advantage of a strain in which LD biogenesis could be controlled through transcriptional induction of the TAG synthase *LRO1* (*GAL-LRO1 are1*Δ *are2*Δ *dga1*Δ) (Jacquier *et al.*, 2011). Prior to galactose-induced formation of LDs, the PLIN3-based reporters stained crescent-like ER domains where Erg6-mCherry was also enriched, indicating that Erg6 is also targeted to these structures, possibly as early stages of LD assembly (Fig. 4E, F). In the control cells, which do not express Wbp1-GFP-PLIN3 or Sec61-GFP-PLIN3, Erg6-mCherry displayed uniform ER localization in cells lacking LDs and rapidly stained ER-localized punctate structures representing LDs, when their biosynthesis was

induced by expression of Lro1 (Jacquier *et al.*, 2011). After 1 h of Lro1 induction, the crescent-like patches formed by Wbp1-GFP-PLIN3 and Sec61-GFP-PLIN3 appeared to dissolve to become more circular/punctuate in case of Wbp1-GFP-PLIN3, or more uniformly distributed in the ER, as observed with Sec61-GFP-PLIN3 (Fig. 4E, F). After overnight induction of LD formation, both Wbp1-GFP-PLIN3 and Sec61-GFP-PLIN3 colocalized with Erg6-mCherry at LDs (Fig. 4E, F).

We have previously shown that Nem1 colocalizes with the LD biogenesis factor seipin at sites in the ER where neutral lipids are formed and LD biogenesis occurs (Choudhary *et al.*, 2020). Given that the ER-crescents formed by the membrane proximal PLIN display hallmarks of sites of LD biogenesis, even in the absence of TAG and STE, we wondered whether seipin would also localize to these crescents. To test this, we induced the expression of mScarlet-PLIN3-tagged Wbp1 or Sec61 in quadruple mutant cells coexpressing GFP-tagged seipin (Fld1-GFP). Prior to expression of the membrane proximal PLIN3, seipin displayed a dispersed punctuated localization (Fig. 4G, H). After overnight induction of Wbp1-mScarlet-PLIN3 or Sec61-mScarlet-PLIN3, the presence of one or several seipin-positive puncta within these crescent-like structures were observed, suggesting that these crescents resemble sites of LD biogenesis in the ER membrane (Fig. 4G, H).

Appending PLIN3 to the ER-luminal side of an integral ER membrane protein leads to its targeting to LDs

Given that appendage of PLIN3 to the cytosolically oriented end of an integral ER membrane proteins such as Wbp1 or Sec61 conveys them to LDs, we wondered whether the LD-localization of these reporters, could be explained by wrapping of the ER membrane around LDs rather than actual localization of the reporters on LDs, as schematically depicted in Fig. 5A. This ER enwrapping-based localization of the reporters on LDs, however, could occur only if the PLIN3 domain is exposed to the cytosol, as is the case with the two reporters studied so far. We thus tested whether fusion of PLIN3 to the luminal domain of a multi-spanning ER membrane protein, would still result in LD localization of the reporter protein. Localization of a membrane reporter containing an ER luminal PLIN3 to a cytosolic LD could not be explained by ER enwrapping. We chose to fuse GFP-PLIN3 to the C-terminus of Pmt1, a multi-spanning ER protein required for protein O-mannosylation, which has a topology that places its C-terminus in the ER lumen (Strahl-Bolsinger and Scheinost, 1999) (Fig. 5B).

When Pmt1-GFP-PLIN3 subcellular distribution was analyzed by fluorescence microscopy, we found that this chimera localized to Nile Red-positive LDs (Fig. 5C). This observation was confirmed by colocalization of Pmt1-GFP-PLIN3 with Erg6-mCherry at the surface of LDs in cells grown in the presence of oleic acid (Fig. 5C). ER luminal exposure of an LD-targeting determinant is thus able to target a protein to LDs. This observation is consistent with our previous report showing that the targeting of GFP-PLIN3 into the ER luminal space by appendage of an N-terminal signal peptide, results in its LD localization (Mishra *et al.*, 2016). The localization of Pmt1-GFP-PLIN3 was not due to a topologically wrong insertion into the ER membrane, because this chimera fractionated with microsomal membranes and the GFP-PLIN3 domain was properly localized to the ER lumen as GFP was protected from protease digestion (Fig. 5D, E). Moreover, Pmt1-GFP-PLIN3 was enriched on isolated LDs, consistent with the localization observed by microscopy (Fig. 5F). In cells lacking LDs, the Pmt1-based reporter displayed a uniform ER localization and colocalized with the ER marker mCherry-HDEL (Fig. 5G). Finally, Pmt1-GFP-PLIN3 was stable and detected as full-length protein on Western blots, indicating that we monitored the entire fusion protein and not a fragment of it (Fig. 5H). Altogether the results obtained with Pmt1-GFP-PLIN3 reveal that LDs are accessible to proteins from both the cytosolic side as well as from the ER luminal space.

We next checked whether like in yeast, an ER luminal PLIN3 is also able to target integral membrane proteins to LDs in mammalian cells. To this end, we appended GFP-PLIN3 to POMT1, a human O-mannosyltransferase orthologue of yeast Pmt1 (Jurado *et al.*, 1999). When transfected into HEK293 cells, POMT1-GFP-PLIN3 extensively colocalized with Nile Red-stained LDs (Fig. 5I). When grown in the presence of oleic acid, POMT1-GFP-PLIN3 localized to the rim of these LDs and its signal overlapped with that of mCherry-PLIN2 (Fig. 5I, J). Thus, an ER luminal orientation of the LD-targeting domain promotes the redistribution of integral ER membrane proteins to LDs in both yeast and mammalian cells. LD localization of these membrane-anchored reporters thus cannot simply be explained by enwrapping of ER around cytosolic LDs as schematically shown in Fig. 5A, but is more likely due to localization of the integral membrane protein either very close to or directly on LDs.

FITs affect access of the ER luminal PLIN3 to LDs

Next, we wondered whether the Wbp1-GFP-PLIN3, Sec61-GFP-PLIN3 and Pmt1-GFP-PLIN3 reporters can be targeted only to newly formed LDs, i.e., target LDs while they are being formed in the ER, or whether they would also be targeted to mature LDs. Therefore, we grew cells expressing Erg6-mCherry in oleic acid-containing medium to induce large LDs, but keeping the expression of the reporters repressed by adding doxycycline. Cells were then switched to medium lacking doxycycline to induce expression of the reporter and their localization was analyzed over time by fluorescence microscopy. Induction of either Wbp1-GFP-PLIN3 or Sec61-GFP-PLIN3 in cells containing pre-existing LDs initially resulted in an arc-like LD rim staining of these reporter after 2 and 4 h of induction (Fig. 6A). Upon prolonged induction of the reporters, this arc-like LD rim staining was superseded by a more uniform staining of the LD perimeter (Fig. 6A). Induction of the reporter containing an ER luminally oriented PLIN3, Pmt1-GFP-PLIN3, in contrast, did not result in its targeting to pre-existing LDs (Fig. 6A). Instead, Pmt1-GFP-PLIN3 appeared to localize to the cell periphery, possibly the cortical ER. These results indicate that the targeting of these membrane-anchored reporters to pre-existing LDs differs, depending on whether the LD targeting signal provided by PLIN3 has a cytosolic or an ER luminal orientation.

To analyze these differences in LD targeting in more detail, we examined the localization of these reporter constructs in FIT mutant cells. FIT proteins are required for the emergence of LDs towards the cytosol (Kadereit *et al.*, 2008; Choudhary *et al.*, 2015). The yeast genome encodes two FIT isoforms, *SCS3* and *YFT2*. In the *scs3*Δ *yft2*Δ double mutant, Wbp1-GFP-PLIN3 and Sec61-GFP-PLIN3 initially labelled LDs only partially, in an arc-like manner, before dispersing over the entire LD perimeter, following the same kinetics as observed in a wild-type background (Fig. 6B). However, unlike in wild-type cells, in the FIT double mutant, Pmt1-GFP-PLIN3 was properly localized to LDs even at early time points (Fig. 6B). These results suggest that the FIT proteins regulate access of membrane-anchored reporters to LDs. Thus, in the presence of functional FIT proteins, the membrane-anchored reporter containing an ER luminal LD-targeting domain, Pmt1-GFP-PLIN3, failed to properly localize to pre-existing LDs. However, in the absence of FIT protein function, Pmt1-GFP-PLIN3 could distribute to pre-existing LDs. The function of FIT proteins in controlling access of Pmt1-GFP-PLIN3 to mature LDs is redundant because the two single mutants, *yft2*Δ and *scs3*Δ, behaved as wild-type cells and prevented targeting of Pmt1-GFP-PLIN3 to pre-existing LDs (Fig. S2A, B). While FIT function affected targeting of Pmt1-GFP-

PLIN3 to the rim of pre-existing LDs, it did not affect the stability of the protein, as revealed by a cycloheximide chase Western blot analysis (Fig. S2C). Based on these observations and as proposed before (Choudhary *et al.*, 2015), we favor the hypothesis that FIT proteins regulate access of ER luminal determinants to pre-existing LDs and/or the topology of the LDs budding, i.e., their emergence towards the cytosol or the ER lumen as depicted in the model shown in Fig. 6C.

Endogenous integral membrane proteins localize to LDs

Given that the results of this study indicate that mono- and polytopic ER membrane proteins localize to the limiting membrane of LDs if fused to a LDs-targeting domain, we wondered whether there are endogenous LD-localized proteins that have multiple transmembrane domains. By combining information from yeast protein localization databases, proteins found to be present in LDs by mass spectrometry, and a topological prediction algorithm (Topcons; (Tsirigos *et al.*, 2015)), we identified at least 2 proteins with multiple transmembrane domains that could reside in LDs. The first is Cst26/Psi1, an acyltransferase that incorporates very long-chain fatty acids into phosphatidylinositol (Le Guédard *et al.*, 2009; Vazquez *et al.*, 2016). This protein has at least 4-6 predicted transmembrane domains and was identified on LDs in a high throughput GFP localization study and by proteomic analysis of isolated LDs (Huh *et al.*, 2003; Grillitsch *et al.*, 2011) (Fig. 7A). The second is Rrt8, a protein implicated in outer spore wall assembly and sterol-dependent transport of membrane proteins, which has 4-6 predicted transmembrane domains and was assigned to LDs by both GFP-localization and mass spectrometry (Huh *et al.*, 2003; Grillitsch *et al.*, 2011; Lin *et al.*, 2013; Ueno *et al.*, 2016) (Fig. 7A).

To confirm the subcellular distribution of these two polytopic integral membrane proteins, we colocalized them with Erg6-mCherry. Remarkably, both of these proteins colocalize with Erg6-mCherry at the surface of LDs (Fig. 7B, C). Moreover, both Cst26 and Rrt8 fractionate with microsomal membranes and they biochemically behave as integral membrane proteins, i.e., they become soluble only upon detergent treatment of membranes (Fig. 7D, E). Finally, both proteins are enriched in isolated LDs (Fig. 7F). These observations thus show that native polytopic membrane proteins can be localized to the surface of LDs, suggesting that the ER membrane is continuous with the limiting membranes of LDs.

Discussion

The results described in this study are twofold and indicate that (i) polytopic membrane proteins can be localized over LDs and that (ii) perilipins, when appended to a membrane anchor, induce the formation of membrane domains that resemble those of early stages of LD biogenesis.

The prevalent model of LD biogenesis postulates that LD formation is driven by the formation of neutral lipids in the ER. These neutral lipids then condense to form lenses within the ER membrane which in turn are recognized by LD biogenetic proteins, including seipin and perilipins (Walther *et al.*, 2017; Olzmann and Carvalho, 2018). These factors then define the sites in the ER where LDs would further grow and mature to eventually bud towards the cytosolic compartment, enclosed by a phospholipid monolayer, but possibly still attached to the ER membrane through a neck composed of seipin oligomers and possibly additional factors (Yan *et al.*, 2018; Salo *et al.*, 2019). FIT proteins and additional parameters such as surface tension, phospholipid synthesis and composition are important to impose a directionality to the budding process hence ensuring emergence of the LD towards the cytosol and not the ER lumen (Choudhary *et al.*, 2015, 2018; Joshi *et al.*, 2018; Wang *et al.*, 2018; Chorlay *et al.*, 2019). In the absence of FIT proteins or if surface tensions are altered, LDs emerge towards the ER lumen, thereby topologically resembling the biogenesis of lipoproteins (Choudhary *et al.*, 2015; Chorlay *et al.*, 2019).

The prevalent model for LD biogenesis proposes that either the cytosolic or the luminal half of the ER membrane enwraps the neutral lipid core of the LD providing for continuity of an ER hemimembrane with the surface monolayer of the LD (Fig. 7G). This membrane continuity would facilitate the relocation of proteins with a hairpin-type of membrane anchor from the ER bilayer onto the LD monolayer. But would the continuity of this hemimembrane also allow integral membrane proteins to move between an ER bilayer and an LD monolayer? This may be an option for dedicated proteins, such as possibly LDAF1/Promethin, a polytopic membrane protein which is closely associated with seipin and relocates from the ER to the LD surface upon maturation of LDs (Castro *et al.*, 2019; Chung *et al.*, 2019) }. On the other hand, for non-dedicated ER residential membrane proteins as used in this study, i.e., Sec61 and Wbp1, it is difficult to imagine how they could relocate from a bilayer environment to the limiting membrane of LDs. The observation that induction of these reporters initially results in their accumulation in crescent-shaped LD domains, before they

distribute over the entire LD surface, indicates that the transfer of these proteins on the LD perimeter is slow (Fig. 6A). Whether this transfer requires an adaptation of the protein to an altered membrane environment or an adaptation of the LD surface to the presence of these proteins, however, cannot be resolved based on the data provided in this study.

One model to account for the observed localization of integral membrane proteins on LDs would be if LDs were partially or even completely surrounded by a normal bilayer membrane, i.e., the ER bilayer. In that case, LDs could be held in place by the ER membrane in an "egg cup" arrangement, as proposed based on a freeze-fracture electron microscopy (EM) study (Robenek *et al.*, 2006). Alternatively, LDs might even be completely enclosed by the ER membrane and thus be positioned in the ER lumen, as are lipoproteins, and as with lipoproteins, their hydrophobic core could still be enclosed by a lipid monolayer (Tauchi-Sato *et al.*, 2002) (Fig. 7G). Such ER luminal LDs might be tightly wrapped by the ER membrane and essentially constitute an ER domain that is recognized by dedicated LD-localized proteins. The fact that the wrapping of an ER bilayer around a luminal LD is not routinely observed by EM speaks against this possibility. However, EM analyses relies on heavily processed samples, including crosslinking, dehydration, resin embedding, and contrasting, and material that does not crosslink well, such as saturated lipids or neutral lipids, may be difficult to preserve (Fujimoto *et al.*, 2013). However, ER luminal LDs are observed in cells with a block in lipoprotein assembly (Ohsaki *et al.*, 2008). While ER luminal LDs could provide a possible explanation for the observed targeting of integral membrane proteins to the surface of LDs, much more additional evidence is needed to further support or disqualify this model.

The second interesting result of this study is the observation that membrane proximal PLINs form crescent-like structures in quadruple mutant cells lacking TAG and STE (Fig. 4). These structures bear the hallmarks of early stages of LD assembly as they can be stained with Nile Red, are enriched in LD-localized proteins such as Erg6 and even recruit seipin, one of the earliest known factors that organizes LD biogenesis in the ER (Salo *et al.*, 2019; Choudhary *et al.*, 2020). These findings are interesting because they indicate that perilipins not only recognize cues that are specific to the monolayer of LDs but they also recognize possibly similar cues in the ER bilayer. These cues are likely lipid-dependent and it has been proposed that perilipins and particularly their repeats of amphipathic helices detect lipid packaging defects

(Bulankina *et al.*, 2009; Copic *et al.*, 2018; Prévost *et al.*, 2018; Chorlay and Thiam, 2020). Such lipid packing defects could be induced by the presence of low levels of neutral lipids, including TAG, STE but possibly also DAG, within the LD monolayer but maybe also within the ER bilayer. These neutral lipids are soluble in a membrane bilayer at low concentration and could possibly even diffuse from the core of a luminal LD into the surrounding ER bilayer as depicted in Fig. 7G thereby providing a lipid-identity cue to this particular ER domain to mark it as an "LD" (Hamilton, 1989). Protein at the ER neck such as seipin, FIT proteins or possibly LDAF may ensure that these lipid-identity cues, i.e. the neutral lipids, do not diffuse into the bulk of the ER bilayer.

Overall, the results of this study indicate that natively occurring multispanning integral membrane proteins can localize to the rim of LDs in both yeast and mammalian cells. These results thus indicate that the LD surface is accessible not only to cytosolic proteins containing amphipathic helices, or membrane proteins containing a hairpin type of topology but also to polytopic integral membrane proteins. This suggests that the ER bilayer membrane into which these proteins are first inserted is continuous with the surface membrane of LDs. Further studies are now needed to understand how the presence of such polytopic integral membrane proteins on the LD surface can be reconciled with the prevalent view that the LDs perimeter is composed of a membrane monolayer.

Acknowledgements

We thank all members of the lab for support, advice and helpful discussions, Vineet Choudhary and Aslihan Ekim for comments on the manuscript, Mykhaylo Debelyy for analyzing protein topologies, Claire Jacob for advice on the construction of mammalian expression vectors and Mert Duman for preliminary localization experiments. F.R. is supported by ZonMW TOP (91217002), ALW Open Programme (ALWOP.310) and H2020 Marie Skłodowska-Curie Actions Cofund (713660) and Marie Skłodowska Curie ETN (765912) grants. M.M. is supported by an ALW Open Programme (ALWOP.355). R.S. is supported by the Swiss National Science Foundation (31003A_17303) and the Novartis Foundation for medical-biological Research (19B140).

Conflicts of Interests

The authors declare to have no conflicts of interests.

Materials and Methods

Yeast strains, media and growth conditions

Yeast strains and their genotype are listed in supplementary Table S1. Heterozygous diploid deletion strains in BY4743 background were obtained from Thermo Fisher Scientific (Waltham, MA). Diploid strains were sporulated on SPO media (0.022% raffinose and 0.3% calcium acetate) at 24°C and dissected using a micromanipulator (Singer Instruments, Somerset, UK). Yeast strains were cultured in YP-rich medium [1% bacto yeast extract, 2% bacto peptone (USBiological, Swampscott, MA)] or selective medium [0.67% yeast nitrogen base without amino acids (USBiological), 0.73 g/l amino acids)], containing either 2% glucose or 2% galactose. Fatty acid-supplemented medium contained 0.24% Tween 40 (Sigma-Aldrich, St Louis, MO) and 0.12% oleic acid (Carl Roth, Karlsruhe, Germany). Synthesis of fatty acids and sterols was inhibited by the addition of cerulenin (10 µg/ml; Enzo Life Sciences, Inc., Farmingdale, NY) and terbinafine (30 µg/ml), respectively. To repress expression of the fusion constructs, cells were cultivated in the presence of doxycycline 1 µg/ml; Sigma-Aldrich, St Louis, MO). Expression was then induced by shifting cells to media lacking doxycycline, typically 14 h before imaging.

Yeast expression constructs

Plasmid pCM189 containing the tetracycline-repressible *tetO*$_7$ promoter (Garí *et al.*, 1997) was used as a backbone to express the fusion proteins listed in the supplementary Table S2. The plasmid was linearized with BamHI and PstI, and a PCR fragment containing GFP-PLIN3 was inserted by homologous recombination in yeast (Hua *et al.*, 1997), resulting in pCM189-GFP-PLIN3. pCM189-GFP-PLIN3 was then linearized by PacI and fragments encoding *WBP1*, *SEC61* and *PMT1*, PCR-amplified from the yeast genomic DNA, were inserted by homologous recombination in yeast, resulting in Wbp1-GFP-PLIN3, Sec61-GFP-PLIN3, and Pmt1-GFP-PLIN3. To generate pCM189-mScarlet, the DNA encoding for mScarlet was codon optimized for expression in yeast and chemically synthesized (GenScript, Piscataway, NJ). mScarlet was then PCR amplified and cloned as a PstI/BamHI fragment into the pCM189 plasmid. Plasmids expressing Wbp1-mScarlet and Sec61-mScarlet were constructed by amplifying *WBP1* and *SEC61* followed by cloning into PacI-digested pCM189-

mScarlet. All constructs were verified by sequencing (Microsynth AG, Buchs, Switzerland).

Mammalian cell culture and expression constructs

Human embryonic kidney HEK293 cells were obtained from ATCC (Manassas, VA). Cells were cultured in DMEM (PAN-Biotech GmbH, Aidenbach, Germany) supplemented with 10% (v/v) fetal bovine serum (VWR International GmbH) and 0.2% penicillin-streptomycin (PAN-Biotech). Cells were seeded in 6-well plates and transfected the following day using lipofectamine 3000 (Thermo Fisher Scientific). 20 mM oleic acid complexed with 2.5 mM BSA were added to cells 16 h post transfection. Cells were incubated with oleic acid for 4 h prior to imaging. mCherry-PLIN2 expressed from the pLENTI6-mCherry-PLIN2 vector was used to label LDs (Eyre *et al.*, 2014). SEC61A1-GFP-PLIN3 (Sino Biological, cDNA clone 19659-UT) and POMT1-GFP-PLIN3 (Sino Biological, cDNA clone 17179-UT) were cloned into pLENTI6 as NheI/FspI and NheI/ScaI fragments, respectively. OST48-GFP-PLIN3 (Sino Biological, cDNA clone 12463-UT) was cloned within the ScaI/NotI sites of pSiCoR-GFP-EF1α (Jacob *et al.*, 2014). All constructs were verified by sequencing (Microsynth AG, Buchs, Switzerland).

Protein fractionation and Western blot analysis

To analyse the subcellular distribution of the fusion proteins by fractionation, exponentially growing cells were harvested by centrifugation. Cells were then lysed in lysis buffer (20 mM HEPES pH 6.8, 150 mM potassium acetate, 250 mM Sorbitol, 1 mM DTT, 250 mM $MgCl_2$, 2 mM PMSF and protease inhibitors (Roche Diagnostics, Mannheim, Germany)) by disruption with glass beads. The cell homogenate was cleared by centrifugation at 3,000 g for 5 min and then separated into pellet (P13) and supernatant (S13) fractions by centrifugation at 13,000 *g* for 30 min at 4°C. The S13 fraction was further separated into (P30) and supernatant (S30) fractions by centrifugation at 30,000 *g* for 30 min at 4°C. The S30 was finally fractionated at 100,000 *g* for 1 h to yield a high-speed pellet (P100) and the cytosol (S100).

To determine the membrane association of the fusion proteins, 50 µg of proteins from the microsomal membrane pellet (P13) were incubated in lysis buffer containing either 1 M NaCl, 0.1 M Na_2CO_3, or 1% SDS for 30 min on ice. Samples were then centrifuged at 13,000 *g* for 30 min. Proteins in the pellet and the supernatant were

precipitated by trichloroacetic acid (TCA) (10%), resuspended in SDS-PAGE loading buffer and analysed by Western blot.

For proteinase K protection experiments, 50 µg of proteins from the microsomal membrane pellet (P13) were incubated with 30 µg/ml of proteinase K (Roche Diagnostics, Mannheim, Germany) for 30 min on ice. Proteins were precipitated with TCA, and subjected to Western blot analysis.

For deglycosylation, 30 µg of microsomal proteins were treated with EndoH-Hf (New England Biolabs, Ipswich, MA) for 4 h at 37°C. The reaction was stopped by the addition of 1 mM PMSF and proteins were precipitated with 10% TCA. The pellet was dissolved in loading buffer and subjected to Western blot analysis.

LDs were isolated by two consecutive flotations essentially as previously described (Leber *et al.*, 1994). Briefly, spheroplasts were resuspended in lysis buffer (12% Ficoll PM 400, 10 mM MES-Tris, pH 6.9, 0.2 mM EDTA) and the lysate was cleared by centrifugation at 5,000 *g* for 5 min. This homogenate (H) was placed at the bottom of an ultracentrifuge tube, overlaid with lysis buffer and floated by centrifugation at 100,000 *g* for 1 h. The floating fraction was collected, diluted in lysis buffer and placed at the bottom of a second ultracentrifuge tube, which was overlaid with 8% Ficoll in 10 mM MES–Tris, pH 6.9, 0.2 mM EDTA and centrifuged at 100,000 *g* for 1 h. The second floating fraction corresponds to the crude LDs fraction. Proteins were delipidated with diethyl ether, TCA precipitated and analyzed by Western blotting. Protein concentration was determined by the method of Lowry, using the Folin's reagent and BSA as standard.

GFP-fusion proteins were detected using a monoclonal antibody (Roche Diagnostics, diluted at 1:2000, #11814460001). Primary antibodies against Wbp1 (M. Aebi, ETH Zurich, Switzerland, diluted at 1:2000), Kar2 (R. Schekman, University of California, Berkeley, CA, diluted at 1:5000), Ayr1 (G. Daum, TU-Graz, Austria, diluted at 1:5000), or Sec61 (R. Schekman, diluted at 1:2000) were detected by using horseradish peroxidase (HRP)-conjugated secondary antibodies (Santa Cruz Biotechnology, Dallas, TX, diluted at 1:10,000, #sc-2030 and #sc-2302). Western blots and fractionation experiments were repeated at least two times with essentially similar results.

Fluorescence microscopy

Yeast cells were grown to an early logarithmic phase (~1 OD_{600nm}), pelleted by centrifugation and resuspended in a small volume of media. 3 µl of the cell suspension were mounted on a glass slide and covered with an agarose patch. Confocal images were recorded using a Leica TCS SP5 confocal microscope equipped with a 63x/1.20 HCX PL APO objective, and a LAS AF software. Cells were stained with Nile Red (10 µg/ml, Sigma-Aldrich, St Louis, MO) for 5 min at room temperature and washed twice with PBS. Localization of mCherry- and GFP-tagged fusion proteins was performed by fluorescence microscopy of live yeast cells using a Visitron spinning disc CSU-W1 (Visitron Systems, Puchheim Germany) or a DeltaVision deconvolution microscope (Applied Precision, Issaquah, WA). The Visitron spinning disk CSU-W1 consisted of a Nikon Ti-E inverted microscope, equipped with a CSU-W1 spinning disk head with a 50-µm pinhole disk (Yokogawa, Tokyo, Japan), an Evolve 512 (Photometrics) EM-CCD camera, and a PLAN APO 100x NA 1.3 oil objective (Nikon). The Delta Vision Elite (GE Healthcare, Pittsburgh, PA) imaging system consisted of an Olympus 1X71 inverted microscope equipped with a CCD camera (CoolSNAP HQ^2, Photometrics, Tuscon, AZ). Images were acquired using a U PLAN S-APO 100x NA 1.3 oil immersion objective (Olympus). Eleven sections separated by 0.2 µm were deconvolved using the iterative constrained deconvolution program in softWoRx (Applied Precision, GE Healthcare, Pittsburgh, PA).

Mammalian HEK293 cells were cultured in 6-well glass bottom plates (IBL, Gerasdorf, Austria). Cells were imaged 16 h post-transfection with or without oleic acid-treatment using the Visitron spinning disk microscope. Images shown are Z projections of 20-30 stacks collected at a 0.5 µm step interval. Quantification of the GFP and mCherry signals was performed using the Fiji software (Schindelin *et al.*, 2012). For Nile Red staining, cells were incubated with Nile Red (10 µg/ml; Sigma-Aldrich, St Louis, MO) for 5 min at 37°C and washed twice with PBS, before fresh medium was added and images collected using a Leica TCS SP5 (Leica, Wetzlar, Germany). A single confocal section is shown.

Colocalization was evaluated manually by scoring color overlap in 100 lipid droplets (% colabelling per cell). Images were treated using ImageJ software and then resized in Photoshop (Adobe, Mountain View). Microscopic experiments were performed three times with essentially similar results.

Lipid labelling

Neutral lipid synthesis and accumulation were monitored by labeling cells with 10 µCi/ml [^{3}H]palmitic acid (American Radiolabeled Chemicals, St Louis, MO) for the indicated periods of time as previously described (Jacquier and Schneiter, 2010). TAG mobilization was monitored in cells that were labeled overnight with 10 µCi/ml [^{3}H]palmitic acid and then diluted into fresh medium supplemented with cerulenin (10 µg/ml) and terbinafine (30 µg/ml) as described (Köffel *et al.*, 2005). Subsequently, cells were collected and lipids were extracted with chloroform/methanol (1:1; v/v), and aliquots were brought to dryness. Lipids were separated by TLC on silica gel plates (Merck, Darmstadt, Germany), and plates were developed in petroleum ether/diethyl ether/acetic acid (70:30:2; v/v/v). TLC plates were then exposed to a tritium-sensitive screen and visualized using a phosphorimager (Typhoon, GE Healthcare). Lipids were quantified using ImageJ.

Electron microscopy

For immune-electron microscopy, cells were grown in fatty acid supplemented medium at 30°C. Cell aliquots were collected by centrifugation, chemically fixed, embedded in 12% gelatin and cryosectioned as described previously (Griffith *et al.*, 2008). Sections were then immunogold-labeled using a rabbit anti-GFP antiserum (Abcam, Cambridge, UK) and 10 nm protein A–gold, before being viewed in a CM100bio TEM (FEI, Eindhoven, Netherlands).

For the statistical evaluations, the number of LDs per cell section was determined by counting 100 randomly selected cell profiles. The relative distribution of the gold particles was calculated by classifying 550 of them, on the basis of their localization to the ER, LDs and mitochondria. A gold particle was assigned to a compartment when it was situated within 15 nm of the limiting membrane. The linear labeling density and the average organelle surface were established using the point hit method as described previously (Rabouille, 1999; Kondylis and Rabouille, 2003). Standard deviations were used to perform a *t*-test, confirming the statistical significance of the data (P<0.05).

Quantification of ER-LD contacts was performed on three independent grids with a total of 30 random cell profiles for each genotype, using the intersection method (Rabouille, 1999). The relative distribution of the marker proteins was quantified by 4 independent evaluations of random cell profiles over three independent grids counting 682 gold particles for Erg6-GFP, 600 for Wbp1-GFP-PLIN3 and 659 particles for

Sec61-GFP-PLIN3. Gold particles were assigned to a specific compartment, i.e., the ER or LDs, when no further than 15 nm away from its limiting membrane (Mari *et al.*, 2008).

References

Athenstaedt K, Daum G (2000) 1-Acyldihydroxyacetone-phosphate reductase (Ayr1p) of the yeast Saccharomyces cerevisiae encoded by the open reading frame YIL124w is a major component of lipid particles. *J Biol Chem*, **275:** 235–240

Brasaemle DL (2007) Thematic review series: adipocyte biology. The perilipin family of structural lipid droplet proteins: stabilization of lipid droplets and control of lipolysis. *J Lipid Res*, **48:** 2547–2559

Bulankina AV, Deggerich A, Wenzel D, Mutenda K, Wittmann JG, Rudolph MG, Burger KN, Honing S (2009) TIP47 functions in the biogenesis of lipid droplets. *J Cell Biol*, **185:** 641–655

Bussell RJ, Eliezer D (2003) A structural and functional role for 11-mer repeats in alpha-synuclein and other exchangeable lipid binding proteins. *J Mol Biol*, **329:** 763–778

Castro IG, Eisenberg-Bord M, Persiani E, Rochford JJ, Schuldiner M, Bohnert M (2019) Promethin Is a Conserved Seipin Partner Protein. *Cells*, **8:**

Chorlay A, Monticelli L, Veríssimo Ferreira J, Ben M'barek K, Ajjaji D, Wang S, Johnson E, Beck R, Omrane M, Beller M, Carvalho P, Rachid Thiam A (2019) Membrane Asymmetry Imposes Directionality on Lipid Droplet Emergence from the ER. *Dev Cell*, **50:** 25–42.e7

Chorlay A, Thiam AR (2020) Neutral lipids regulate amphipathic helix affinity for model lipid droplets. *Journal of Cell Biology*, **219:**

Choudhary V, El Atab O, Mizzon G, Prinz WA, Schneiter R (2020) Seipin and Nem1 establish discrete ER subdomains to initiate yeast lipid droplet biogenesis. *J Cell Biol*, **219:**

Choudhary V, Golani G, Joshi AS, Cottier S, Schneiter R, Prinz WA, Kozlov MM (2018) Architecture of Lipid Droplets in Endoplasmic Reticulum Is Determined by Phospholipid Intrinsic Curvature. *Curr Biol*, **28:** 915–926.e9

Choudhary V, Ojha N, Golden A, Prinz WA (2015) A conserved family of proteins facilitates nascent lipid droplet budding from the ER. *J Cell Biol*, **211:** 261–271

Chung J, Wu X, Lambert TJ, Lai ZW, Walther TC, Farese RV (2019) LDAF1 and Seipin Form a Lipid Droplet Assembly Complex. *Dev Cell*,

Copic A, Antoine-Bally S, Giménez-Andrés M, La Torre Garay C, Antonny B, Manni MM, Pagnotta S, Guihot J, Jackson CL (2018) A giant amphipathic helix from a perilipin that is adapted for coating lipid droplets. *Nat Commun*, **9:** 1332

Deshaies RJ, Schekman R (1987) A yeast mutant defective at an early stage in import of secretory protein precursors into the endoplasmic reticulum. *J Cell Biol*, **105:** 633–645

Dhiman R, Caesar S, Thiam AR, Schrul B (2020) Mechanisms of protein targeting to lipid droplets: A unified cell biological and biophysical perspective. *Semin Cell Dev Biol*,

Eyre NS, Fiches GN, Aloia AL, Helbig KJ, McCartney EM, McErlean CS, Li K, Aggarwal A, Turville SG, Beard MR (2014) Dynamic imaging of the hepatitis C virus NS5A protein during a productive infection. *J Virol*, **88:** 3636–3652

Fujimoto T, Ohsaki Y, Suzuki M, Cheng J (2013) Imaging lipid droplets by electron microscopy. *Methods Cell Biol*, **116:** 227–251

Gao Q, Binns DD, Kinch LN, Grishin NV, Ortiz N, Chen X, Goodman JM (2017) Pet10p is a yeast perilipin that stabilizes lipid droplets and promotes their assembly. *J Cell Biol*, **216:** 3199–3217

Garí E, Piedrafita L, Aldea M, Herrero E (1997) A set of vectors with a tetracycline-regulatable promoter system for modulated gene expression in Saccharomyces cerevisiae. *Yeast*, **13:** 837–848

Goh VJ, Tan JS, Tan BC, Seow C, Ong WY, Lim YC, Sun L, Ghosh S, Silver DL (2015) Postnatal Deletion of Fat Storage-inducing Transmembrane Protein 2 (FIT2/FITM2) Causes Lethal Enteropathy. *J Biol Chem*, **290:** 25686–25699

Görlich D, Prehn S, Hartmann E, Kalies KU, Rapoport TA (1992) A mammalian homolog of SEC61p and SECYp is associated with ribosomes and nascent polypeptides during translocation. *Cell*, **71:** 489–503

Griffith J, Mari M, De Maziere A, Reggiori F (2008) A cryosectioning procedure for the ultrastructural analysis and the immunogold labelling of yeast Saccharomyces cerevisiae. *Traffic*, **9:** 1060–1072

Grillitsch K, Connerth M, Kofeler H, Arrey TN, Rietschel B, Wagner B, Karas M, Daum G (2011) Lipid particles/droplets of the yeast Saccharomyces cerevisiae revisited: lipidome meets proteome. *Biochim Biophys Acta*, **1811:** 1165–1176

Grippa A, Buxó L, Mora G, Funaya C, Idrissi FZ, Mancuso F, Gomez R, Muntanyà J, Sabidó E, Carvalho P (2015) The seipin complex Fld1/Ldb16 stabilizes ER-lipid droplet contact sites. *J Cell Biol*, **211:** 829–844

Gross DA, Zhan C, Silver DL (2011) Direct binding of triglyceride to fat storage-inducing transmembrane proteins 1 and 2 is important for lipid droplet formation. *Proc Natl Acad Sci U S A*, **108:** 19581–19586

Hamilton JA (1989) Interactions of triglycerides with phospholipids: incorporation into the bilayer structure and formation of emulsions. *Biochemistry*, **28:** 2514–2520

Hua SB, Qiu M, Chan E, Zhu L, Luo Y (1997) Minimum length of sequence homology required for in vivo cloning by homologous recombination in yeast. *Plasmid*, **38:** 91–96

Huh WK, Falvo JV, Gerke LC, Carroll AS, Howson RW, Weissman JS, O'Shea EK (2003) Global analysis of protein localization in budding yeast. *Nature*, **425:** 686–691

Jacob C, Lötscher P, Engler S, Baggiolini A, Varum Tavares S, Brügger V, John N, Büchmann-Møller S, Snider PL, Conway SJ, Yamaguchi T, Matthias P, Sommer L, Mantei N, Suter U (2014) HDAC1 and HDAC2 control the specification of neural crest cells into peripheral glia. *J Neurosci*, **34:** 6112–6122

Jacquier N, Choudhary V, Mari M, Toulmay A, Reggiori F, Schneiter R (2011) Lipid droplets are functionally connected to the endoplasmic reticulum in Saccharomyces cerevisiae. *J Cell Sci*, **124:** 2424–2437

Jacquier N, Mishra S, Choudhary V, Schneiter R (2013) Expression of oleosin and perilipins in yeast promotes formation of lipid droplets from the endoplasmic reticulum. *J Cell Sci*, **126:** 5198–5209

Jacquier N, Schneiter R (2010) Ypk1, the yeast orthologue of the human serum- and glucocorticoid-induced kinase, is required for efficient uptake of fatty acids. *J Cell Sci*, **123:** 2218–2227

Joshi AS, Nebenfuehr B, Choudhary V, Satpute-Krishnan P, Levine TP, Golden A, Prinz WA (2018) Lipid droplet and peroxisome biogenesis occur at the same ER subdomains. *Nat Commun*, **9:** 2940

Jurado LA, Coloma A, Cruces J (1999) Identification of a human homolog of the Drosophila rotated abdomen gene (POMT1) encoding a putative protein O-mannosyl-transferase, and assignment to human chromosome 9q34.1. *Genomics*, **58:** 171–180

Kadereit B, Kumar P, Wang WJ, Miranda D, Snapp EL, Severina N, Torregroza I, Evans T, Silver DL (2008) Evolutionarily conserved gene family important for fat storage. *Proc Natl Acad Sci U S A*, **105:** 94–99

Kassan A, Herms A, Fernandez-Vidal A, Bosch M, Schieber NL, Reddy BJ, Fajardo A, Gelabert-Baldrich M, Tebar F, Enrich C, Gross SP, Parton RG, Pol A (2013) Acyl-CoA synthetase 3 promotes lipid droplet biogenesis in ER microdomains. *J Cell Biol*, **203:** 985–1001

Khandelia H, Duelund L, Pakkanen KI, Ipsen JH (2010) Triglyceride blisters in lipid bilayers: implications for lipid droplet biogenesis and the mobile lipid signal in cancer cell membranes. *PLoS One*, **5:** e12811

Köffel R, Tiwari R, Falquet L, Schneiter R (2005) The Saccharomyces cerevisiae YLL012/YEH1, YLR020/YEH2, and TGL1 genes encode a novel family of membrane-anchored lipases that are required for steryl ester hydrolysis. *Mol Cell Biol*, **25:** 1655–1668

Kondylis V, Rabouille C (2003) A novel role for dp115 in the organization of tER sites in Drosophila. *J Cell Biol*, **162:** 185–198

Kory N, Farese RV, Walther TC (2016) Targeting Fat: Mechanisms of Protein Localization to Lipid Droplets. *Trends Cell Biol*, **26:** 535–546

Le Guédard M, Bessoule JJ, Boyer V, Ayciriex S, Velours G, Kulik W, Ejsing CS, Shevchenko A, Coulon D, Lessire R, Testet E (2009) PSI1 is responsible for the stearic acid enrichment that is characteristic of phosphatidylinositol in yeast. *FEBS J*, **276:** 6412–6424

Leber R, Zinser E, Zellnig G, Paltauf F, Daum G (1994) Characterization of lipid particles of the yeast, Saccharomyces cerevisiae. *Yeast*, **10:** 1421–1428

Lin CP, Kim C, Smith SO, Neiman AM (2013) A highly redundant gene network controls assembly of the outer spore wall in S. cerevisiae. *PLoS Genet*, **9:** e1003700

Mari M, Bujny MV, Zeuschner D, Geerts WJ, Griffith J, Petersen CM, Cullen PJ, Klumperman J, Geuze HJ (2008) SNX1 defines an early endosomal recycling exit for sortilin and mannose 6-phosphate receptors. *Traffic*, **9:** 380–393

Markgraf DF, Klemm RW, Junker M, Hannibal-Bach HK, Ejsing CS, Rapoport TA (2014) An ER protein functionally couples neutral lipid metabolism on lipid droplets to membrane lipid synthesis in the ER. *Cell Rep*, **6:** 44–55

Mishra S, Khaddaj R, Cottier S, Stradalova V, Jacob C, Schneiter R (2016) Mature lipid droplets are accessible to ER luminal proteins. *J Cell Sci*, **129:** 3803–3815

Mishra VK, Palgunachari MN, Segrest JP, Anantharamaiah GM (1994) Interactions of synthetic peptide analogs of the class A amphipathic helix with lipids. Evidence for the snorkel hypothesis. *J Biol Chem*, **269:** 7185–7191

Murphy DJ, Vance J (1999) Mechanisms of lipid-body formation. *Trends Biochem Sci*, **24:** 109–115

Ohsaki Y, Cheng J, Suzuki M, Fujita A, Fujimoto T (2008) Lipid droplets are arrested in the ER membrane by tight binding of lipidated apolipoprotein B-100. *J Cell Sci*, **121:** 2415–2422

Olzmann JA, Carvalho P (2018) Dynamics and functions of lipid droplets. *Nat Rev Mol Cell Biol*, **20:** 137–155

Omasits U, Ahrens CH, Müller S, Wollscheid B (2014) Protter: interactive protein feature visualization and integration with experimental proteomic data. *Bioinformatics*, **30:** 884–886

Prévost C, Sharp ME, Kory N, Lin Q, Voth GA, Farese RV, Walther TC (2018) Mechanism and Determinants of Amphipathic Helix-Containing Protein Targeting to Lipid Droplets. *Dev Cell*, **44:** 73–86.e4

Rabouille C (1999) Quantitative aspects of immunogold labeling in embedded and nonembedded sections. *Methods Mol Biol*, **117:** 125–144

Robenek H, Hofnagel O, Buers I, Robenek MJ, Troyer D, Severs NJ (2006) Adipophilin-enriched domains in the ER membrane are sites of lipid droplet biogenesis. *J Cell Sci*, **119:** 4215–4224

Roboti P, High S (2012) The oligosaccharyltransferase subunits OST48, DAD1 and KCP2 function as ubiquitous and selective modulators of mammalian N-glycosylation. *J Cell Sci*, **125:** 3474–3484

Rowe ER, Mimmack ML, Barbosa AD, Haider A, Isaac I, Ouberai MM, Thiam AR, Patel S, Saudek V, Siniossoglou S, Savage DB (2016) Conserved Amphipathic Helices Mediate Lipid Droplet Targeting of Perilipins 1-3. *J Biol Chem*, **291:** 6664–6678

Salo VT, Belevich I, Li S, Karhinen L, Vihinen H, Vigouroux C, Magré J, Thiele C, Hölttä-Vuori M, Jokitalo E, Ikonen E (2016) Seipin regulates ER-lipid droplet contacts and cargo delivery. *EMBO J*, **35:** 2699–2716

Salo VT, Li S, Vihinen H, Hölttä-Vuori M, Szkalisity A, Horvath P, Belevich I, Peränen J, Thiele C, Somerharju P, Zhao H, Santinho A, Thiam AR, Jokitalo E, Ikonen E (2019) Seipin Facilitates Triglyceride Flow to Lipid Droplet and Counteracts Droplet Ripening via Endoplasmic Reticulum Contact. *Dev Cell*,

Sandager L, Gustavsson MH, Stahl U, Dahlqvist A, Wiberg E, Banas A, Lenman M, Ronne H, Stymne S (2002) Storage lipid synthesis is non-essential in yeast. *J Biol Chem*, **277:** 6478–6482

Schindelin J, Arganda-Carreras I, Frise E, Kaynig V, Longair M, Pietzsch T, Preibisch S, Rueden C, Saalfeld S, Schmid B, Tinevez JY, White DJ, Hartenstein V, Eliceiri K, Tomancak P, Cardona A (2012) Fiji: an open-source platform for biological-image analysis. *Nat Methods*, **9:** 676–682

Strahl-Bolsinger S, Scheinost A (1999) Transmembrane topology of pmt1p, a member of an evolutionarily conserved family of protein O-mannosyltransferases. *J Biol Chem*, **274:** 9068–9075

Sui X, Arlt H, Brock KP, Lai ZW, DiMaio F, Marks DS, Liao M, Farese RV, Walther TC (2018) Cryo-electron microscopy structure of the lipid droplet-formation protein seipin. *J Cell Biol*, **217:** 4080–4091

Szymanski KM, Binns D, Bartz R, Grishin NV, Li WP, Agarwal AK, Garg A, Anderson RG, Goodman JM (2007) The lipodystrophy protein seipin is found at endoplasmic reticulum lipid droplet junctions and is important for droplet morphology. *Proc Natl Acad Sci U S A*, **104:** 20890–20895

Tauchi-Sato K, Ozeki S, Houjou T, Taguchi R, Fujimoto T (2002) The surface of lipid droplets is a phospholipid monolayer with a unique Fatty Acid composition. *J Biol Chem*, **277:** 44507–44512

te Heesen S, Janetzky B, Lehle L, Aebi M (1992) The yeast WBP1 is essential for oligosaccharyl transferase activity in vivo and in vitro. *EMBO J*, **11:** 2071–2075

Thiam AR, Dugail I (2019) Lipid droplet-membrane contact sites - from protein binding to function. *J Cell Sci*, **132:**

Thiam AR, Farese RVJ, Walther TC (2013) The biophysics and cell biology of lipid droplets. *Nat Rev Mol Cell Biol*, **14:** 775–786

Thiam AR, Forêt L (2016) The physics of lipid droplet nucleation, growth and budding. *Biochim Biophys Acta*, **1861:** 715–722

Tsirigos KD, Peters C, Shu N, Käll L, Elofsson A (2015) The TOPCONS web server for consensus prediction of membrane protein topology and signal peptides. *Nucleic Acids Res*, **43:** W401–7

Ueno K, Nagano M, Shimizu S, Toshima JY, Toshima J (2016) Lipid droplet proteins, Lds1p, Lds2p, and Rrt8p, are implicated in membrane protein transport associated with ergosterol. *Biochem Biophys Res Commun*, **475:** 315–321

Vazquez HM, Vionnet C, Roubaty C, Mallela SK, Schneiter R, Conzelmann A (2016) Chemogenetic E-MAP in Saccharomyces cerevisiae for Identification of Membrane Transporters Operating Lipid Flip Flop. *PLoS Genet*, **12:** e1006160

Walther TC, Chung J, Farese RV (2017) Lipid Droplet Biogenesis. *Annu Rev Cell Dev Biol*, **33:** 491–510

Wang S, Idrissi FZ, Hermansson M, Grippa A, Ejsing CS, Carvalho P (2018) Seipin and the membrane-shaping protein Pex30 cooperate in organelle budding from the endoplasmic reticulum. *Nat Commun*, **9:** 2939

Wild R, Kowal J, Eyring J, Ngwa EM, Aebi M, Locher KP (2018) Structure of the yeast oligosaccharyltransferase complex gives insight into eukaryotic N-glycosylation. *Science*, **359:** 545–550

Wilfling F, Wang H, Haas JT, Krahmer N, Gould TJ, Uchida A, Cheng JX, Graham M, Christiano R, Frohlich F, Liu X, Buhman KK, Coleman RA, Bewersdorf J, Farese

RVJ, Walther TC (2013) Triacylglycerol synthesis enzymes mediate lipid droplet growth by relocalizing from the ER to lipid droplets. *Dev Cell*, **24:** 384–399

Wolins NE, Rubin B, Brasaemle DL (2001) TIP47 associates with lipid droplets. *J Biol Chem*, **276:** 5101–5108

Xu N, Zhang SO, Cole RA, McKinney SA, Guo F, Haas JT, Bobba S, Farese RVJ, Mak HY (2012) The FATP1-DGAT2 complex facilitates lipid droplet expansion at the ER-lipid droplet interface. *J Cell Biol*, **198:** 895–911

Yan R, Qian H, Lukmantara I, Gao M, Du X, Yan N, Yang H (2018) Human SEIPIN Binds Anionic Phospholipids. *Dev Cell*, **47:** 248–256.e4

Zehmer JK, Bartz R, Bisel B, Liu P, Seemann J, Anderson RG (2009) Targeting sequences of UBXD8 and AAM-B reveal that the ER has a direct role in the emergence and regression of lipid droplets. *J Cell Sci*, **122:** 3694–3702

Figure Legends

Figure 1. Membrane-anchored reporters localize to the rim of LDs.

A) Schematic structure of the membrane-anchored reporter proteins used in this study. The ER resident protein Wbp1 containing a single transmembrane domain, or the translocon subunit Sec61, containing multiple transmembrane domains, were fused to a reporter and targeting cassette consisting of GFP and perilipin 3 (PLIN3), a mammalian LD targeted protein. The green barrel indicates GFP, transmembrane domains are shown by orange cylinders, neutral lipids (TAG and STE) by yellow fills.

B) Localization of Wbp1-GFP-PLIN3 and Sec61-GFP-PLIN3 to LDs in wild-type cells. Cells were grown in rich medium overnight at 30°C in the absence of doxycycline to induce expression of the reporters. Cells were stained with Nile Red and analyzed by confocal microscopy. White arrowheads indicate colocalization on LDs. BF, Bright field. Bar, 5 µm.

C) Quantification of colocalization of Wbp1-GFP-PLIN3, Sec61-GFP-PLIN3, and GFP-PLIN3 with Nile Red stained LDs. N>100 LDs.

D) Wbp1-GFP-PLIN3 and Sec61-GFP-PLIN3 colocalize with Erg6-mCherry at the rim of LDs. Cells were cultivated in media containing oleic acid (0.12%) and the subcellular localization of -GFP and -mCherry tagged reporters was analyzed by fluorescence microscopy. A scan of fluorescence intensity along the white line that crosses two adjacent LDs is shown to the right. Bar, 2.5 µm.

E) Quantification of colocalization of Wbp1-GFP-PLIN3, Sec61-GFP-PLIN3, and GFP-PLIN3 with Erg6-mCherry labelled LDs. N>100 LDs.

F) Wbp1-GFP-PLIN3 and Sec61-GFP-PLIN3 are stable. Total cell extracts from wild-type cells expressing either Wbp1-GFP-PLIN3 or Sec61-GFP-PLIN3 were analyzed by Western blotting. The membrane was probed with antibodies against GFP and the ER luminal chaperone Kar2.

G) Wbp1-GFP-PLIN3 and Sec61-GFP-PLIN3 are enriched on isolated LDs. LDs were isolated by flotation on step density gradients and an equal amount of protein (10 µg) from the homogenate (H) and the isolated LD fraction were probed by Western blotting using antibodies against GFP, and the LD-localized protein Ayr1.

H) Wbp1-GFP-PLIN3 and Sec61-GFP-PLIN3 cofractionate with membranes. Cells were fractionated by differential centrifugation and individual fractions were probed by Western blotting using antibodies against GFP and either native Wbp1 or Sec61. H,

homogenate; P13, 13,000 *g* pellet; P30, 30,000 *g* pellet; P100, 100,000 *g* pellet; S100, 100,000 *g* supernatant.

I) Wbp1-GFP-PLIN3 and Sec61-GFP-PLIN3 become solubilized by detergent treatment only. Microsomal membranes were treated with salt (1 M NaCl), carbonate (0.1 M), or SDS (1%) for 30 min on ice, proteins were separated into membrane pellet and supernatant fraction, TCA precipitated, and probed with antibodies against GFP, Kar2, and Wbp1 or Sec61 to detect the native proteins.

J) Wbp1-GFP-PLIN3 is N-glycosylated. Microsomal membranes were treated or not with endoglycosidase H (EndoH), TCA precipitated and analyzed by Western blotting to detect Wbp1-GFP-PLIN3 or the native version of Wbp1.

Figure 2. Immune-EM analysis of the subcellular distribution of the membrane-anchored LD reporters.

A, B, C) Cells expressing Erg6-GFP (A), Wbp1-GFP-PLIN3 (B), or Sec61-GFP-PLIN3 (C) were grown in oleic acid supplemented medium (0.12%). Cells were collected, chemically fixed and processed for cryosectioning and immunogold labelling using an anti-GFP antibody and 10 nm protein A–gold particles indicated by black arrowheads. Organelles are indicated by colors: blue, vacuole; green, lipid droplet; pink, ER adjacent to LD; purple, nucleus. Red square, vesicular-tubular structures. CW, cell wall; ER, endoplasmic reticulum; LD, lipid droplet; M, mitochondria; N, nucleus; PM, plasma membrane; V, vacuole. Scale bar, 0.5 µm.

D) Quantifications of the LD perimeter length enwrapped by the ER membrane and the relative distribution of the respective marker protein between LDs and the ER are shown in the graphs (D).

Figure 3. Integral membrane proteins can localize to LDs in mammalian cells.

A) Colocalization of soluble GFP-PLIN3, membrane-anchored OST48-GFP-PLIN3, and SEC61A1-GFP-PLIN3 with Nile Red stained LDs. Human embryonic kidney cells, HEK293, were transfected with the indicated GFP-tagged reporters, LDs were induced by cultivating cells in oleic acid containing medium for 4 h, and stained with Nile Red. LD labelling is indicated by arrowheads. Bar, 10 µm.

B) Colocalization of soluble GFP-PLIN3, membrane-anchored OST48-GFP-PLIN3, and SEC61A1-GFP-PLIN3 with LDs labelled by mCherry-PLIN2. HEK293 cells were co-transfected with the indicated GFP-tagged reporters and mCherry-PLIN2, LDs were

induced by cultivating cells in oleic acid containing medium for 4 h. Droplets marked by white arrowheads are boxed in the merge and enlarged in the panels to the right. Fluorescent intensity along the white line across the boxed LDs is shown in the graph. Bar, 10 µm.

C, D) Quantification of colocalization of OST48-GFP-PLIN3, SEC61A1-GFP-PLIN3, and GFP-PLIN3 with LDs stained either by Nile Red (C) or labelled with mCherry-PLIN2 (D) in the presence or absence (w/o) of oleic acid. N>100 LDs.

Figure 4. Membrane-anchored PLIN form crescent-like ER membrane domains containing seipin in cells lacking LDs.

A, B) Wbp1-GFP-PLIN3 and Sec61-GFP-PLIN3 localize to ER membrane domains in cells that have no LDs. Quadruple mutant cells (*are1*Δ *are2*Δ *dga1*Δ *lro1*Δ) expressing the ER marker mCherry-HDEL together with Wbp1-GFP-PLIN3 or Sec61-GFP-PLIN3 were analyzed by fluorescence microscopy. Crescent-formation of ER domains by Wbp1-GFP-PLIN3 and Sec61-GFP-PLIN3 is indicated by pink arrowheads. Bar, 5 µm.

C, D) ER-crescents formed by membrane proximal PLIN3 are Nile Red-positive. Quadruple mutant cells expressing Wbp1-GFP-PLIN3 or Sec61-GFP-PLIN3 were stained with Nile Red. Accumulation of the lipophilic dye in crescent like structures labelled with the PLIN3 reporter proteins is indicated by pink arrowheads. Bar, 5 µm.

E, F) Induction of LD formation results in redistribution of Wbp1-GFP-PLIN3 and Sec61-GFP-PLIN3 from their crescent-like ER domains to punctate LDs. An LD-inducible strain (*GAL-LRO1 are1*Δ *are2*Δ *dga1*Δ) expressing the LD marker Erg6-mCherry and either Wbp1-GFP-PLIN3 or Sec61-GFP-PLIN3 was shifted from glucose containing medium to galactose medium for the indicated period of time to induce expression of the TAG synthase Lro1. Crescent-like ER localization of the membrane-anchored LD reporters at time 0 of induction is indicated by pink arrowheads, punctate localization on LDs upon induction for 1 h or overnight (ON) is indicated by white arrowheads. Bar, 5 µm.

G, H) The LD biogenesis factor seipin is recruited into ER-crescents formed by membrane proximal PLIN3. Expression of Wbp1-mScarlet-PLIN3 and Sec61-mScarlet-PLIN3 was induced by the removal of doxycycline (- Doxy) and cells coexpressing GFP-tagged seipin (Fld1-GFP) were analyzed by fluorescence microscopy at the beginning of the induction of the membrane proximal PLIN3 (0 h)

and after overnight induction (ON). Pink arrowheads mark ER-crescents, white arrows point to clusters of seipin. Bar, 5 µm.

Figure 5. ER luminal localization of the LD targeting domain, PLIN3, results in targeting of an integral membrane protein to LDs.

A) Schematic representation illustrating the wrapping of the ER membrane around LDs, which could account for the observed LD localization of membrane-anchored reporters containing a cytosolic LD-targeting domain.

B) Illustration of the topology of a Pmt1-based membrane-anchored reporter containing the LD targeting domain, GFP-PLIN3, within the ER luminal space.

C) Pmt1-GFP-PLIN3 localizes to punctuate LDs and to the rim of LDs. Cells expressing Pmt1-GFP-PLIN3 were stained with Nile Red and analyzed by fluorescence microscopy. Cells coexpressing Pmt1-GFP-PLIN3 and Erg6-mCherry were grown in oleic acid containing media and analyzed by microscopy. Colocalisation between Pmt1-GFP-PLIN3 and Nile Red is indicated by a white arrowhead, N>100 LDs. A line scan across two LDs is shown. Bar, 5 µm.

D) Pmt1-GFP-PLIN3 fractionates with membranes. Cells expressing Pmt1-GFP-PLIN3 were fractionated by differential centrifugation and equal amount of proteins were probed by Western blotting using the ER luminal Kar2 as control. H, homogenate; P13, 13,000 *g* pellet; P30, 30,000 *g* pellet; P100, 100,000 *g* pellet; S100, 100,000 *g* supernatant .

E) The GFP domain of Pmt1-GFP-PLIN3 is protected from proteinase K digestion. Microsomal membranes were treated with proteinase K (Prot. K) in the presence (+) or absence (-) of 0.1% Triton-X100 (TX100), proteins were TCA precipitated and probed with antibodies against GFP or Kar2.

F) Pmt1-GFP-PLIN3 is enriched on isolated LDs. LDs were isolated by flotation on step density gradients and an equal amount of protein (10 µg) from the homogenate (H) and the isolated LD fraction were probed by Western blotting using antibodies against GFP, and the LD-localized protein Ayr1.

G) Pmt1-GFP-PLIN3 is uniformly distributed in the ER membrane in cells lacking LDs. *are1*Δ *are2*Δ *lro1*Δ *dga1*Δ quadruple mutant cells expressing Pmt1-GFP-PLIN3 and the ER marker mCherry-HDEL were analyzed by fluorescence microscopy. Homogenous distribution in the ER is marked by blue arrows. Bar, 5 µm.

H) Pmt1-GFP-PLIN3 is stable. Western blot of total cell extracts from wild-type and quadruple mutant cells expressing Pmt1-GFP-PLIN3. The membrane was probed with antibodies against GFP and the ER luminal Kar2.

I) POMT1-GFP-PLIN3 is localized to the rim of LDs in mammalian cells. HEK293 cells were cotransfected with POMT1-GFP-PLIN3 and mCherry-PLIN2, incubated in media supplemented with or lacking oleic acid for 4 h and imaged. Colocalization is indicated by white arrowheads, and a line scan across the diameter of a single LD, marked in the white box, is plotted. Bar, 10 µm.

J) Degree of colocalization of POMT1-GFP-PLIN3 with LDs stained with Nile Red and with the LD marker mCherry-PLIN2 in cells grown in the presence (+) or absence (-) of oleic acid is plotted in the graph. N>100 LDs.

Figure 6. FIT proteins control access of ER luminal proteins to LDs.

A, B) Localization of membrane anchored reporters to pre-existing LDs. Wild-type and FIT double mutant (*scs3*Δ *yft2*Δ) cells expressing the indicated membrane-anchored LD reporters were cultivated in oleic acid supplemented medium, expression of the membrane proximal PLIN3 reporters was induced at time 0 by removing doxycycline (- Doxy) and their localization was analyzed by confocal microscopy. Orange arrowheads indicate arc-like LD rim labelling of the reporters, white arrowheads depict the presence of the reporters on LD rims, and blue arrows highlight the localization of Pmt1-GFP-PLIN3 in the peripheral ER. Note the LD rim localization of Pmt1-GFP-PLIN3 in the *scs3*Δ *yft2*Δ double mutant, but not wild-type cells. ON, overnight induction. Bar, 5 µm.

C) Model to account for access of Pmt1-GFP-PLIN3 to mature LDs in FIT mutant cells. LDs emerging towards the cytosol as observed in wild-type cells are accessible to reporters containing PLIN3 in the cytosolic space but not to Pmt1-GFP-PLIN3, which contains the LD-targeting domain in the ER lumen. Emergence of LDs towards the ER luminal compartment in FIT mutant cells (*scs3*Δ *yft2*Δ) allows access of Pmt1-GFP-PLIN3 to these luminally oriented mature LDs.

Figure 7. Native polytopic membrane proteins localize to the rim of LDs.

A) The putative membrane topology of Cst26 and Rrt8 as visualized by Protter is shown (Omasits *et al.*, 2014).

B, C) Cells expressing genomically tagged version of the integral membrane proteins Cst26 or Rrt8 together with the LD marker protein Erg6-mCherry in wild-type (B) or quadruple mutant cells (C) were analyzed by fluorescence microscopy. LD rim staining is shown in the blow-up and a line scan across individual LDs is plotted to the right. Blue arrows indicate ER localization. Bar, 5 µm.

D) Cst26 and Rrt8 cofractionate with membranes. Cells were fractionated by differential centrifugation and individual fractions were probed by Western blotting using antibodies against GFP and Kar2. H, homogenate; P13, 13,000 *g* pellet; P30, 30,000 *g* pellet; P100, 100,000 *g* pellet; S100, 100,000 *g* supernatant.

E) Cst26 and Rrt8 are integral membrane proteins. Microsomal membranes were treated with salt (1 M NaCl), carbonate (0.1 M), or SDS (1%) for 30 min on ice, proteins were separated into membrane pellet and supernatant fraction, TCA precipitated, and probed with antibodies against GFP, and Kar2.

F) Cst26 and Rrt8 are enriched on isolated LDs. LDs were isolated by flotation on step density gradients and an equal amount of protein (10 µg) from the homogenate (H) and the isolated LD fraction were probed by Western blotting using antibodies against GFP, and the LD-localized protein Ayr1.

G) Suggested models to account for the localization of integral membrane proteins on LDs. The model shown to the left (I) illustrates an LD that emerges from the ER bilayer towards the cytosol and containing seipin (Fld1) and FIT proteins at the ER-LD interface. The localization of the Wbp1-GFP-PLIN3 reporter within a lipid monolayer is shown. The middle model (II) depicts an “egg cup” configuration of LDs with seipin and Fld1 at the base of the LD and the Wbp1-GFP-PLIN3 reporter in a lipid bilayer environment. The model to the right (III) shows an ER luminal LD with seipin and FIT proteins at the membrane neck and the LD reporter anchored in a bilayer membrane. The presence of neutral lipids within the ER bilayer enclosing the LD is indicated in yellow.

Supplementary Data

Supplementary Figure Legends

Figure S1. LDs containing Wbp1-GFP-PLIN3 or Sec61-GFP-PLIN3 are functional in neutral lipid metabolism.

A) Neutral lipid synthesis in cells expressing membrane-anchored PLIN3 reporter proteins. Yeast cells expressing GFP-PLIN3, Wbp1-GFP-PLIN3 or Sec61-GFP-PLIN3 were incubated with [^{3}H]palmitic acid for the indicated period of time. Cells were poisoned with NaN_3 and NaF and lipids were extracted, separated by TLC and quantified by phosphorimaging. The time-dependent incorporation of [^{3}H]palmitic acid into TAG and STE is plotted. Data represent means ± SD of at least 3 independent determinations.

B) Neutral lipid degradation in cells expressing membrane-anchored PLIN3 reporter proteins. Cells expressing Dga1-GFP, Wbp1-GFP-PLIN3 or Sec61-GFP-PLIN3 were cultivated in the presence of [^{3}H]palmitic acid overnight. Cells were washed and diluted into fresh media containing cerulenin and terbinafine, to inhibit synthesis of fatty acids and ergosterol, respectively. Samples were withdrawn at the indicated time points, lipids were extracted, separated by TLC, and quantified. Data represent means ± SD of at least 3 independent determinations.

C) Mobilization of neutral lipids results in relocalization of Sec61-GFP-PLIN3 from LDs back into the ER membrane. Wild-type cells expressing the ER marker mCherry-HDEL and either Dga1-GFP, Wbp1-GFP-PLIN3, or Sec61-GFP-PLIN3 were incubated with cerulenin and terbinafine for the indicated period of time and the localization of the GFP-tagged LD reporter proteins was monitored by fluorescence microscopy. White arrowheads indicate LD localization, blue arrows point to homogenous ER distribution, and pink arrowheads mark crescent-like structures. Bar, 5 µm.

Figure S2. Scs3 and Yft2 share a redundant function in preventing access of Pmt1-GFP-PLIN3 to LDs.

A, B) One of the FIT proteins is sufficient to prevent localization of the ER luminal reporter to LDs. Cells lacking one of the FIT proteins, either Scs3 (A) or Yft2 (B) expressing the indicated membrane-anchored LD reporters together with Erg6-

mCherry were cultivated in media containing oleic acid and the localization of the reporters was analyzed by confocal microscopy. White arrowheads indicate punctuate LD localization, blue arrows indicate localization in the ER. Bar, 5 µm.

C) Stability of Pmt1-GFP-PLIN3 is not affected in wild-type compared to *scs3*Δ *yft2*Δ double mutant cells. Cells were cultivated in oleic acid supplemented medium, poisoned by the addition of cycloheximide (10 µg/ml), aliquots were removed at the indicated time points and analyzed by Western blotting. Chimeric proteins were detected with antibodies against GFP, and detection of Kar2 serves as loading control. Relative protein stability over time is plotted in the graph.

Supplementary Tables

Table S1. *S. cerevisiae* strains used in this study

Name	*Relevant Genotype*	Source
BY4741	*MATa his3Δ1 leu2Δ0 met15Δ0 ura3Δ0*	Lab collection
RSY 5796	*MATa his3Δ1 leu2Δ0 ura3Δ0 are1::KanMX are2::KanMX dga1::KanMX lro1::KanMX LYS2 MET15*	Lab collection
RSY 5712	*MATα ura3-52 leu2-3,-122 ade2-3 pep4-3 sec61-2*	A. Conzelmann
RSY 6207	*MATa ade2-101 ura3-52 his3Δ200 lys2-801 wbp1-1*	R. Sieber
RSY 3021	*MATα leu2Δ0 lys2Δ0 ura3Δ0 his3Δ1 are1::KanMX are2Δ::KanMX dga1Δ::loxp-HIS GAL1-LRO1::TRP*	Lab collection
RSY 5870	*MATa his3Δ1 leu2Δ0 ura3Δ0 fit2a::KanMX fit2b::KanMX*	Lab collection
RSY 6703	*MATa his3Δ1 leu2Δ0 met15Δ0 ura3Δ0 wbp1::KanMX* pCM189-tetO^7-WBP1	This Study
RSY 6704	*MATa his3Δ1 leu2Δ0 met15Δ0 ura3Δ0 wbp1::KanMX* pCM189-tetO^7-WBP1-GFP	This Study
RSY 6705	*MATa his3Δ1 leu2Δ0 met15Δ0 ura3Δ0 wbp1::KanMX* pCM189-tetO^7-WBP1-GFP-PLIN3	This Study
RSY 6706	*MATa his3Δ1 leu2Δ0 met15Δ0 ura3Δ0 sec61::KanMX* pCM189-tetO^7-SEC61	This Study
RSY 6707	*MATa his3Δ1 leu2Δ0 met15Δ0 ura3Δ0 sec61::KanMX* pCM189-tetO^7-SEC61-GFP	This Study
RSY 6708	*MATa his3Δ1 leu2Δ0 met15Δ0 ura3Δ0 sec61::KanMX* pCM189-tetO^7-SEC61-GFP-PLIN3	This Study
RSY 6664	*MATα his3Δ1 leu2Δ0 lys2Δ0 ura3Δ0 scs3::KanMX*	Euroscarf
RSY 6665	*MATα his3Δ1 leu2Δ0 lys2Δ0 ura3Δ0 yft2::KanMX*	Euroscarf
RSY 6702	*MAT a/α his3Δ1/ his3Δ1 leu2Δ0/ leu2Δ0 ura3Δ0 /ura3Δ0 MET15/ met15Δ0 LYS2/ lys2Δ0 sec61::KanMX/ pSEC61*	Euroscarf
RSY 5837	*MAT a/α his3Δ1/ his3Δ1 leu2Δ0/ leu2Δ0 ura3Δ0 /ura3Δ0 MET15/ met15Δ0 LYS2/ lys2Δ0 wbp1::KanMX/ pWBP1*	Euroscarf
RSY 6371	*MATa his3Δ1 leu2Δ0 met15Δ0 ura3Δ0 FLD1-GFP::HIS3*	Lab collection
RSY 6245	*MATα his3Δ1 leu2Δ0 lys2Δ0 ura3Δ0 ERG6-mCherry::HIS3*	W. Prinz

Table S2. Plasmids used in this study

Plasmids	Source
pCM189-tetO^7-WBP1/ URA3	This Study
pCM189-tetO^7-WBP1-GFP/ URA3	This Study
pCM189-tetO^7-WBP1-GFP-PLIN3/ URA3	This Study
pCM189-tetO^7-SEC61/ URA3	This Study
pCM189-tetO^7-SEC61-GFP/ URA3	This Study
pCM189-tetO^7-SEC61-GFP-PLIN3/ URA3	This Study
pCM189-tetO^7-WBP1-mScarlet-PLIN3/ URA3	This Study
pCM189-tetO^7-SEC61-mScarlet-PLIN3/ URA3	This Study
pCM189-tetO^7-WBP1-mScarlet/ URA3	This Study
pCM189-tetO^7-SEC61-mScarlet/ URA3	This Study
pCM189-tetO^7-WBP1-GFP-PLIN3/ HIS3	This Study
pCM189-tetO^7-SEC61-GFP-PLIN3/ HIS3	This Study
pCM189-tetO^7-PMT1-GFP-PLIN3/ URA3	This Study
pELF1-OST48-GFP-PLIN3	This Study
pCMV-SEC61-GFP-PLIN3	This Study
pCMV-POMT1-GFP-PLIN3	This Study
pRS415-ADH-CST26-GFP/ URA3	This Study
pRS415-ADH-RRT8-GFP/ URA3	This Study
pRS415-ADH-TGL1-GFP/ URA3	This Study
pCM189-tetO^7-WBP1-mScarlet-PLIN1/ URA3	This Study
pCM189-tetO^7-SEC61-mScarlet-PLIN1/ URA3	This Study
pCMV-mCherry-PLIN2	Lab Collection
pGREG505-ADH-ERG6-mCherry/ LEU2	Lab Collection
pRS415-ADH-mCherry-HDEL/ LEU2	Lab Collection
pRS416-ERG6-GFP/ URA3	Lab Collection
pRS416-DGA1-GFP/ URA3	Lab Collection

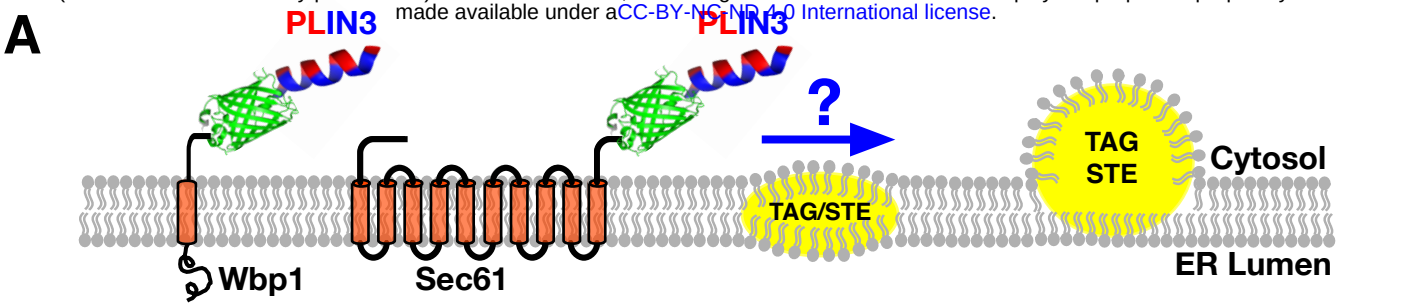

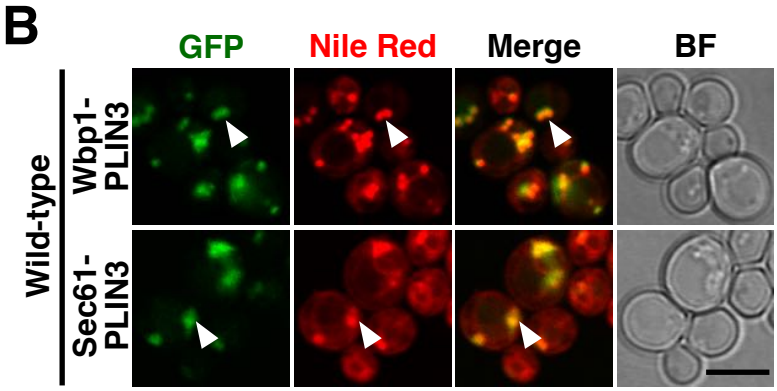

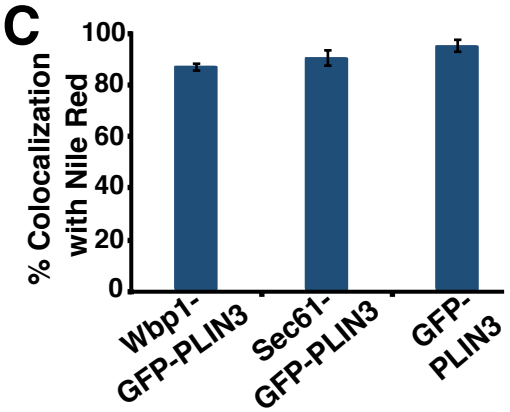

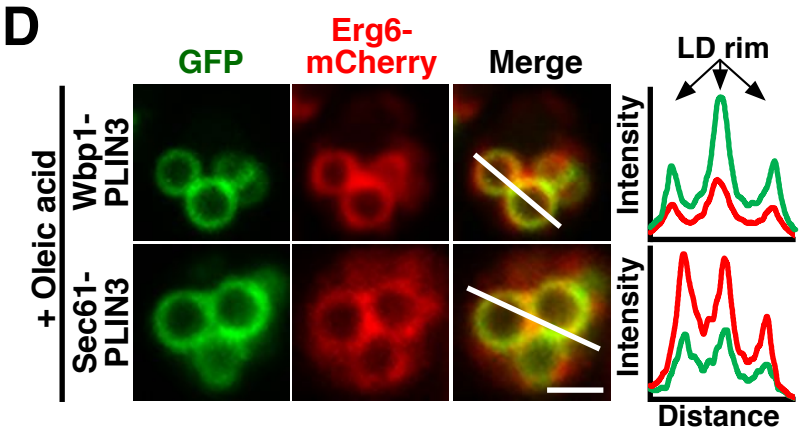

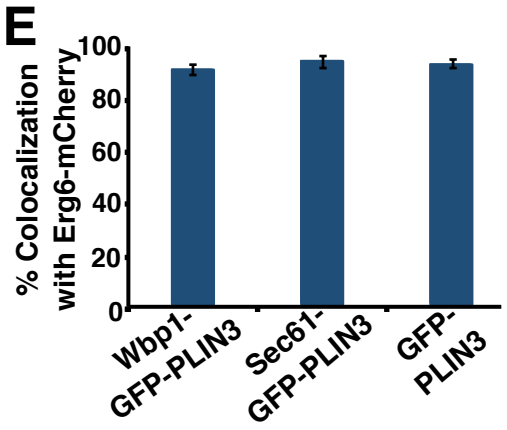

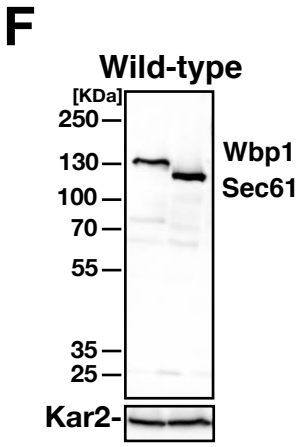

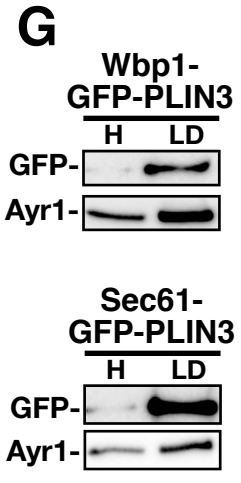

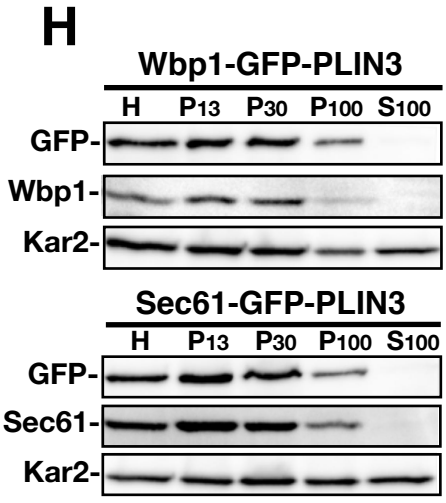

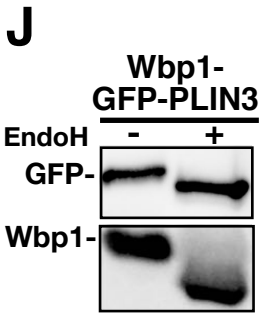

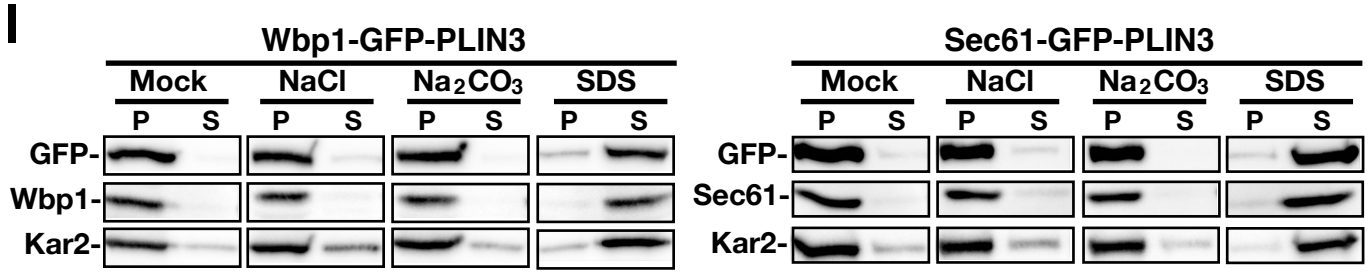

Figure 1

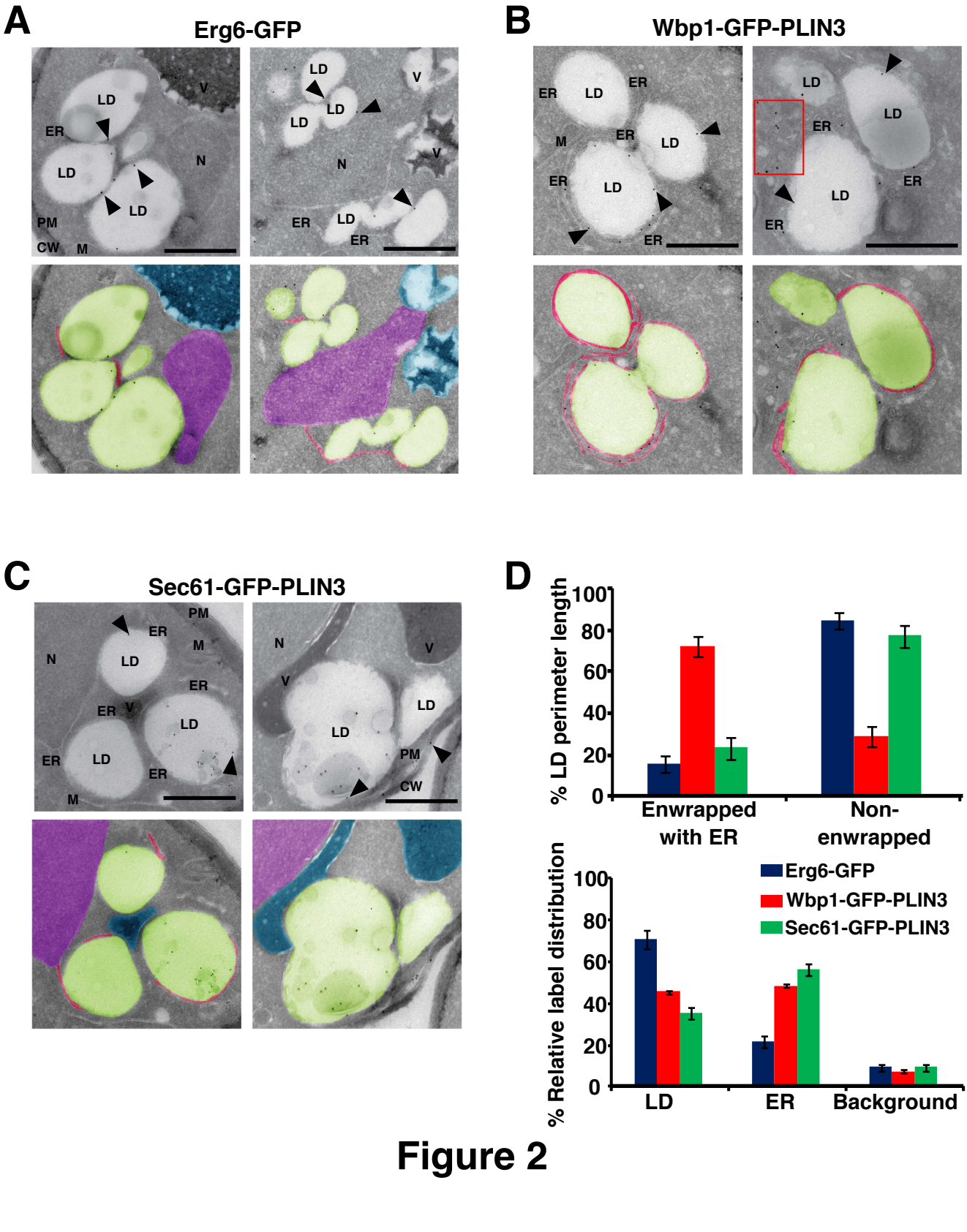

Figure 2

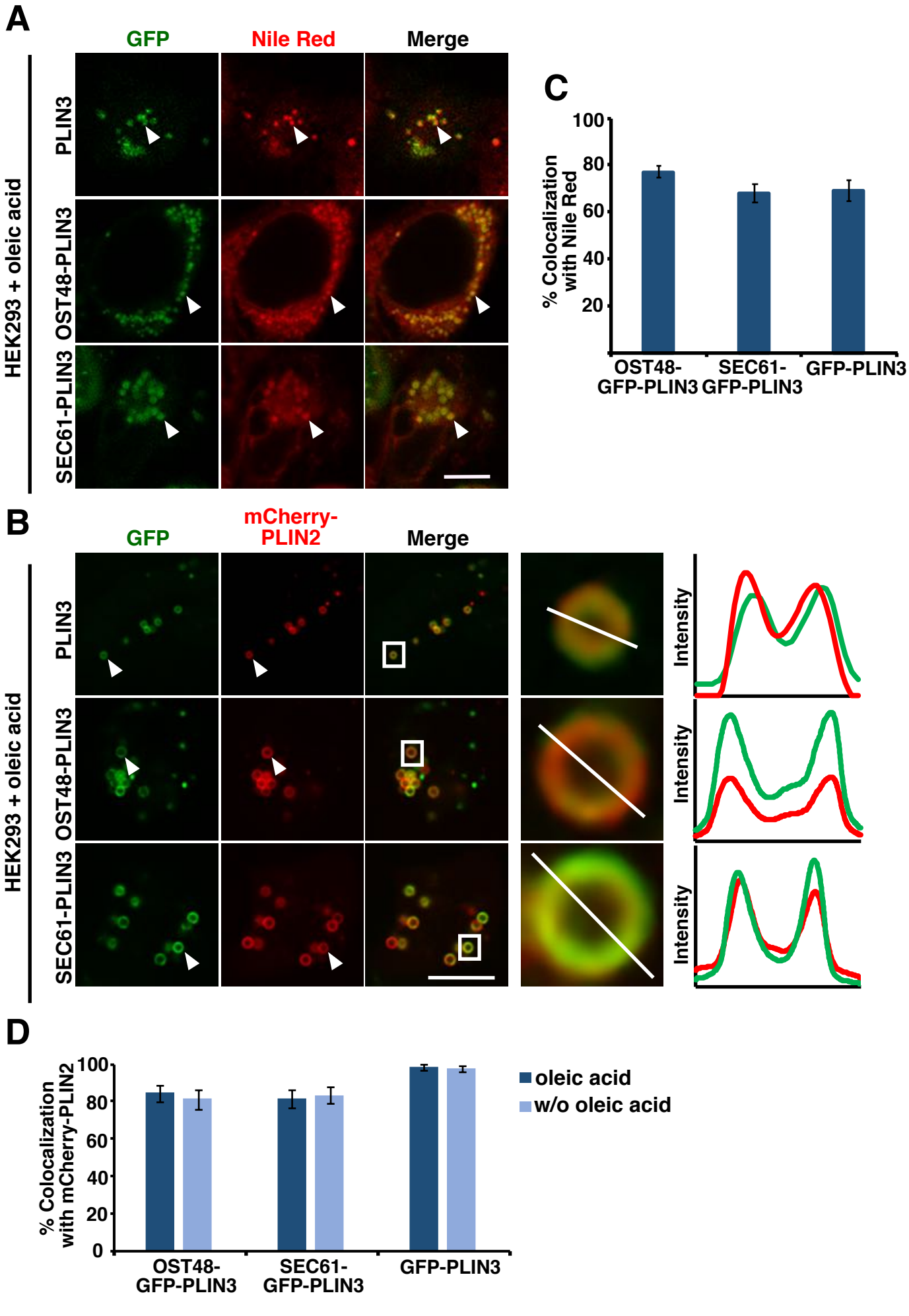

Figure 3

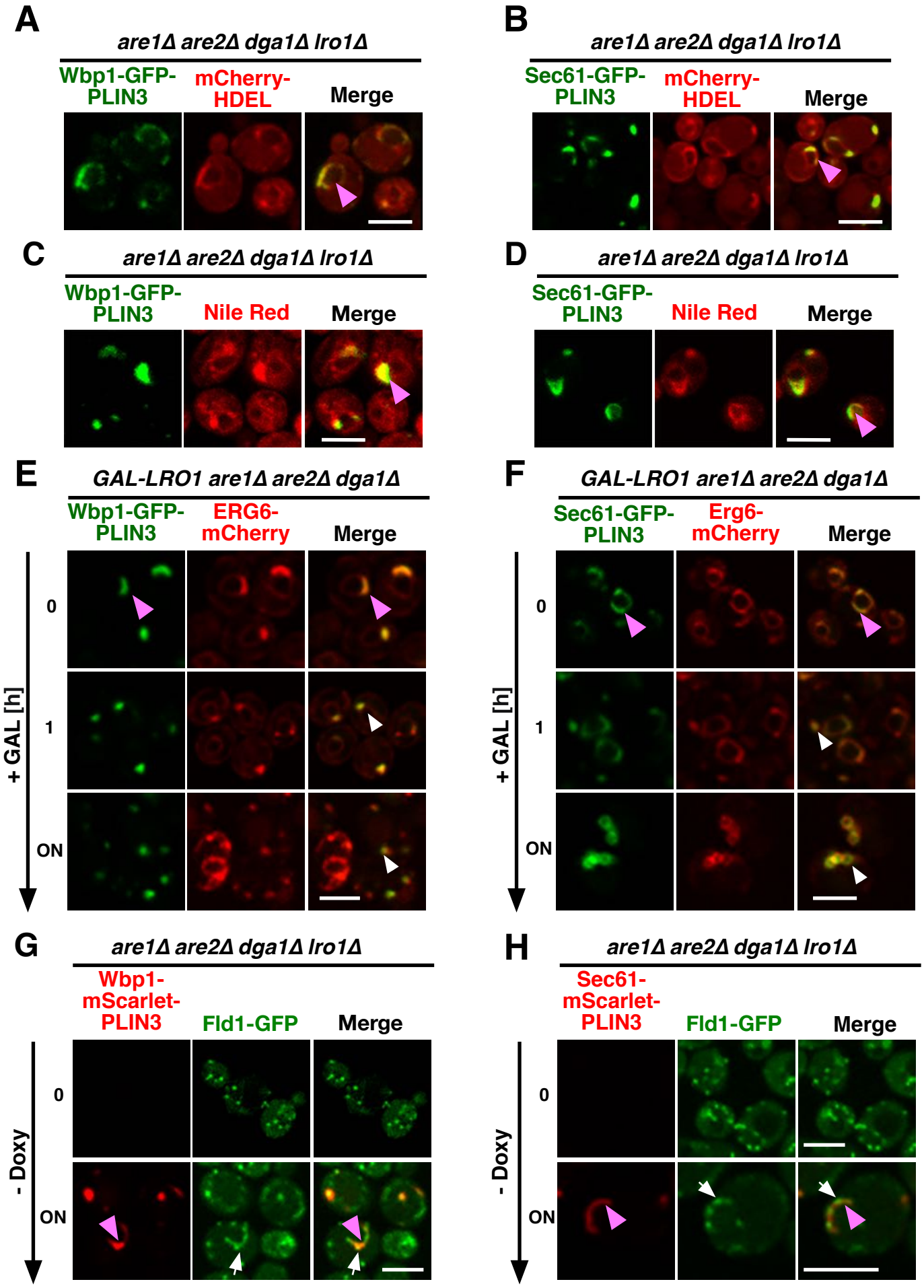

Figure 4

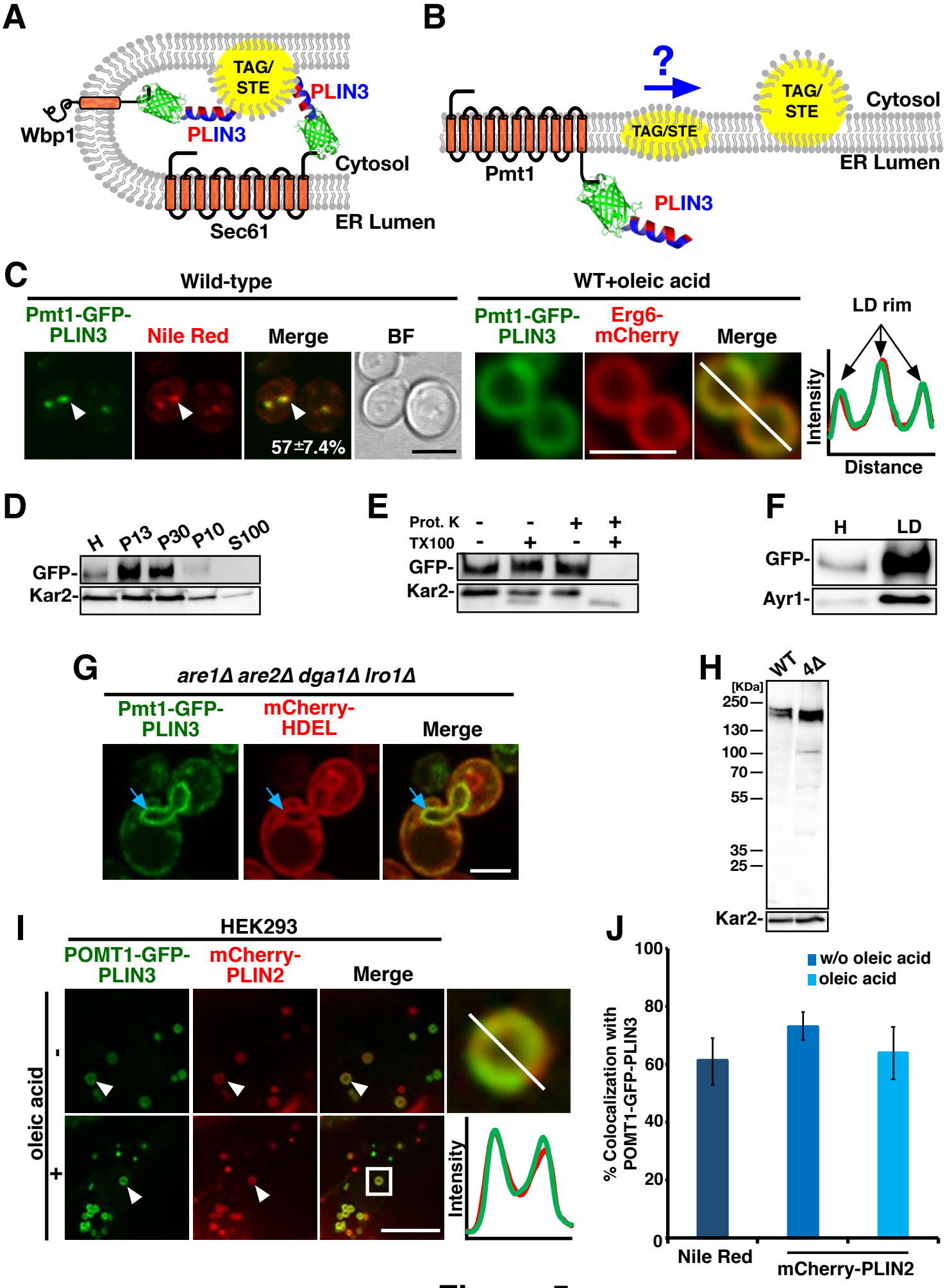

Figure 5

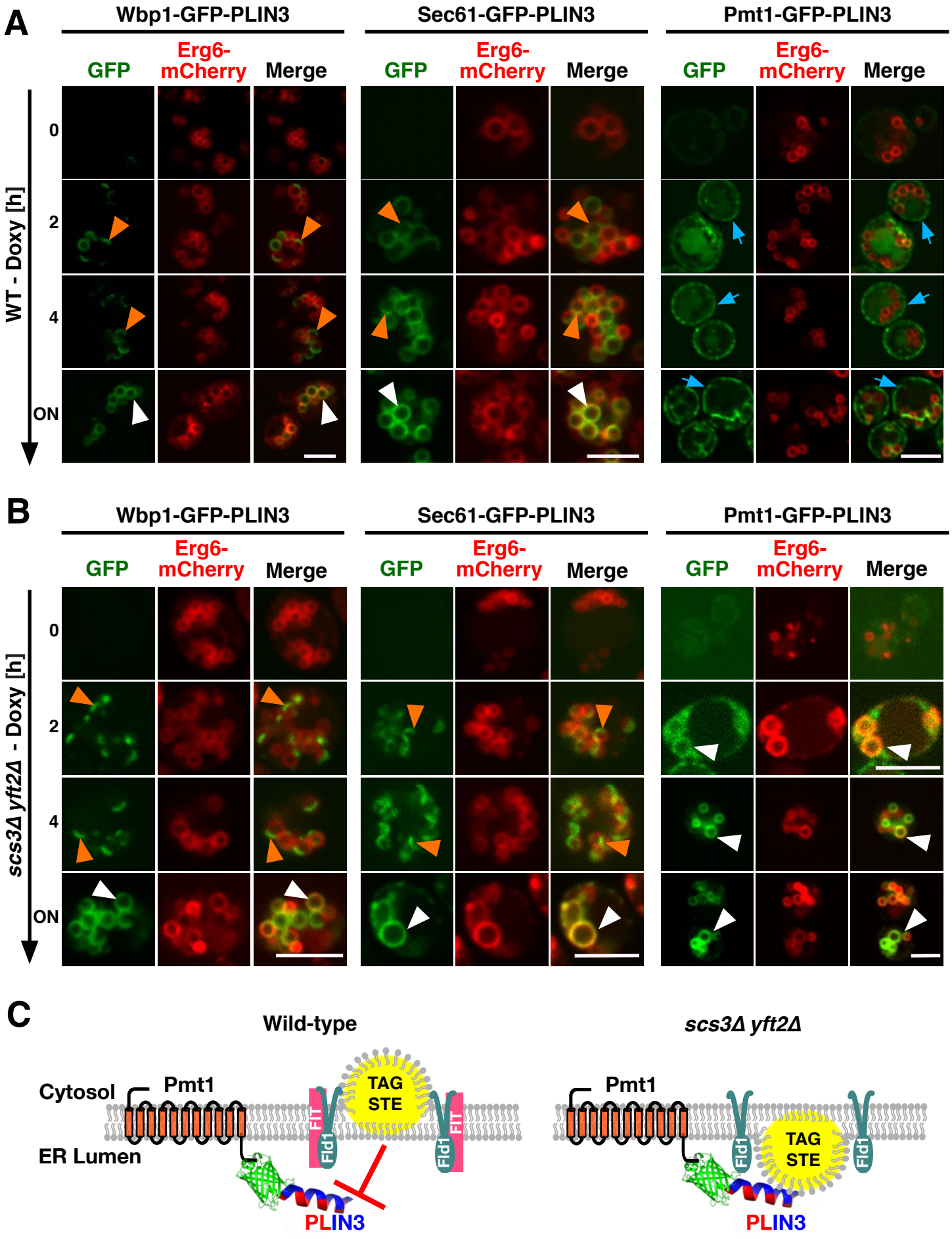

Figure 6

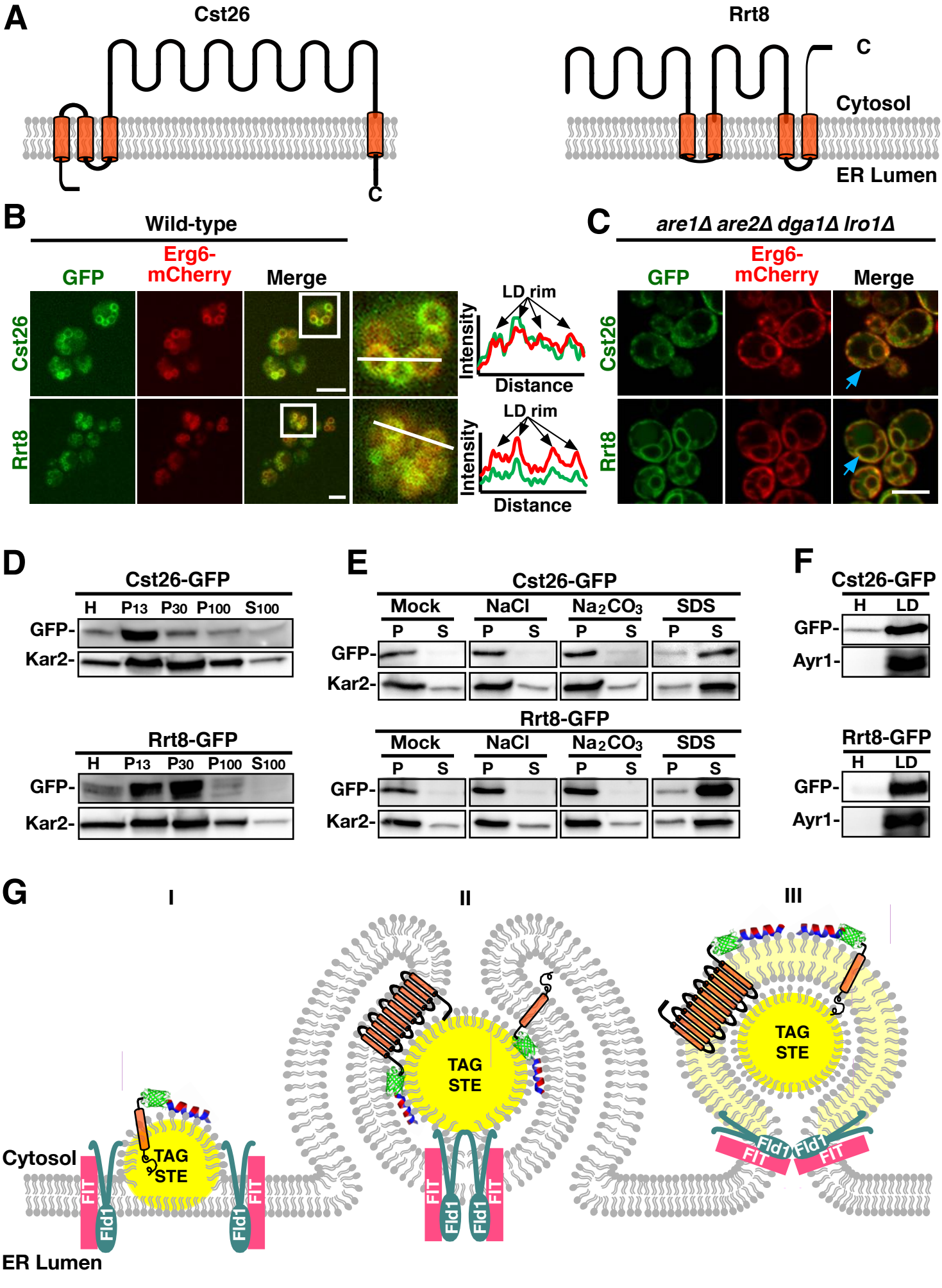

Figure 7

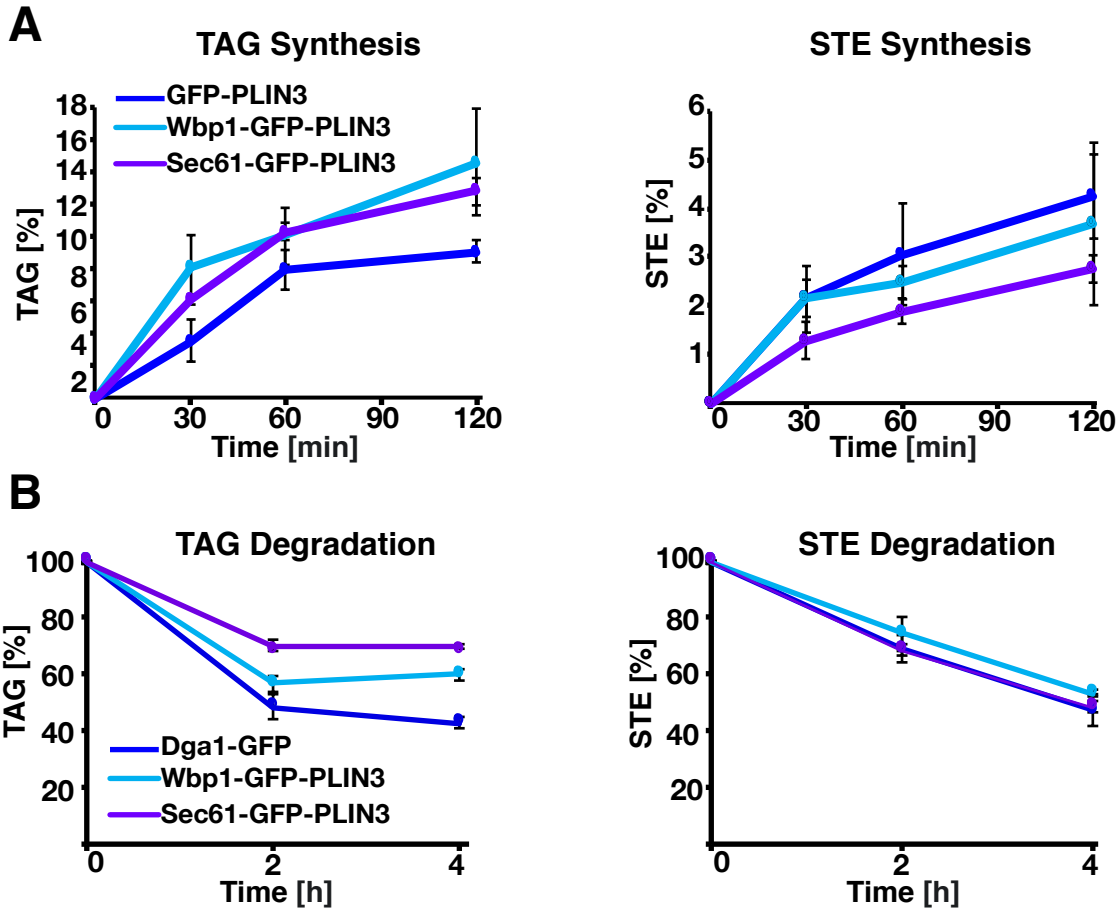

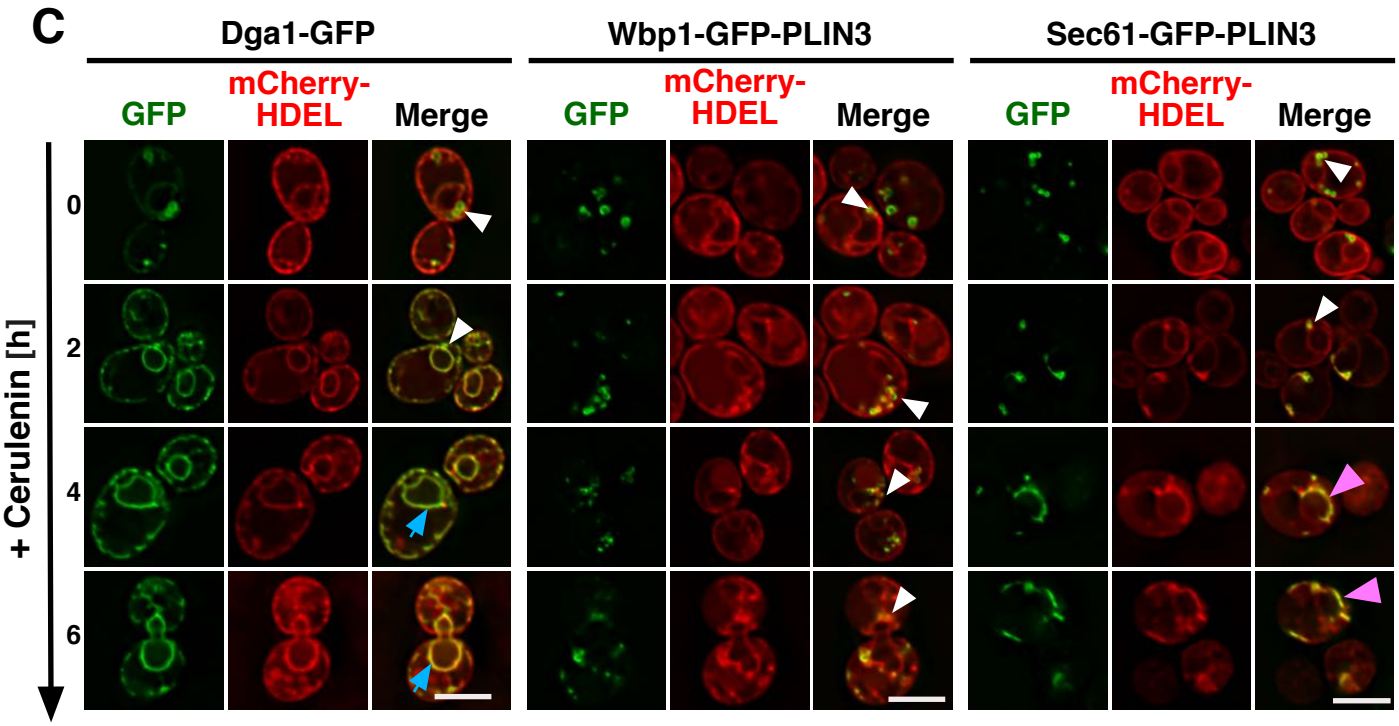

Figure S1

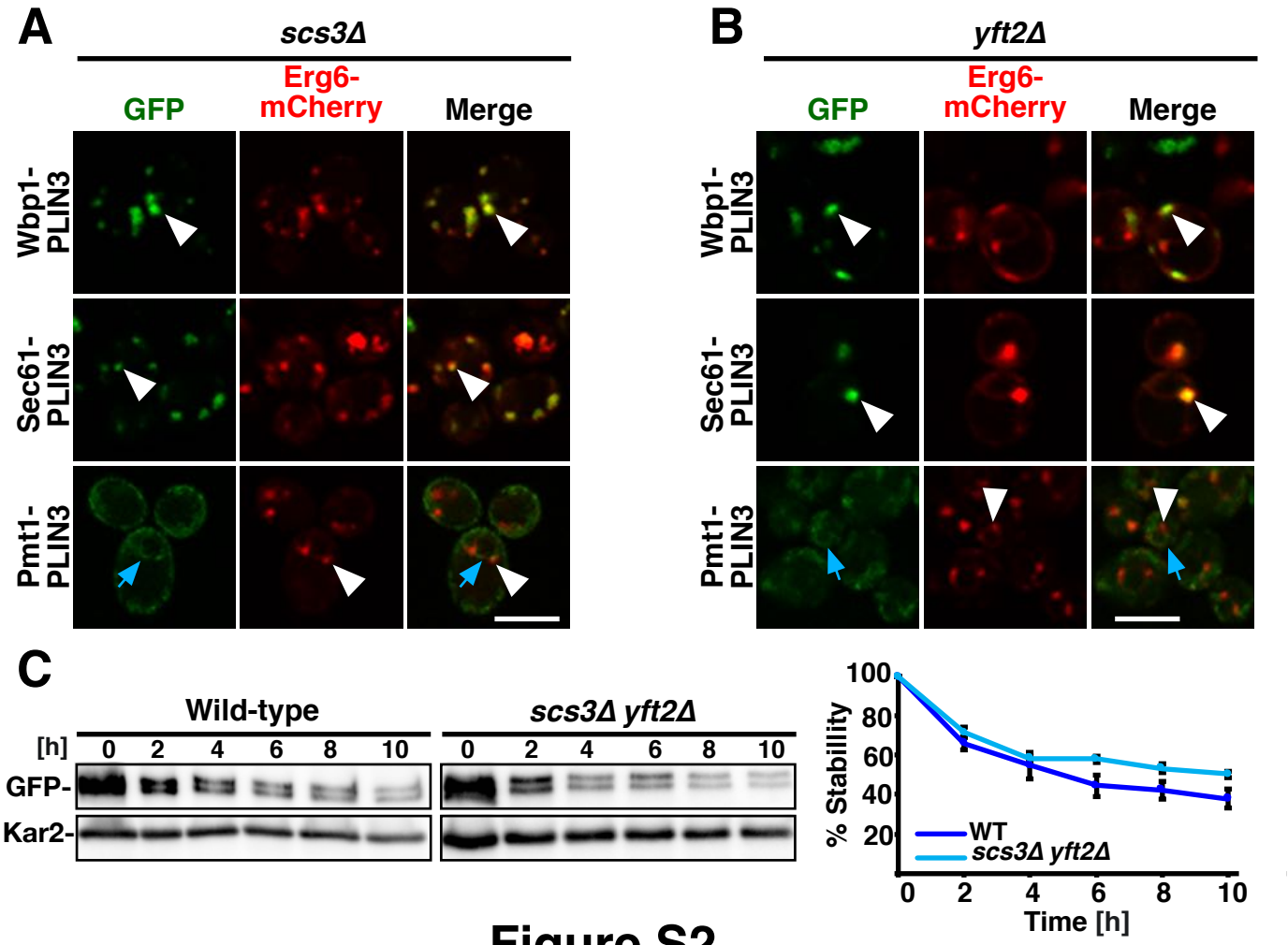

Figure S2